J. Fluid Mech. (2012), *vol.* 712, *pp.* 61–91.
doi:10.1017/jfm.2012.398

Amplitude and frequency modulation in wall turbulence

B. Ganapathisubramani[1]†, N. Hutchins[2], J. P. Monty[2], D. Chung[2] and I. Marusic[2]

[1] Aerodynamics and Flight Mechanics Research Group, University of Southampton, Southampton SO17 1BJ, UK

[2] Department of Mechanical Engineering, University of Melbourne, Melbourne, VIC 3010, Australia

(Received 12 October 2011; revised 1 August 2012; accepted 6 August 2012; first published online 27 September 2012)

In this study we examine the impact of the strength of the large-scale motions on the amplitude and frequency of the small scales in high-Reynolds-number turbulent boundary layers. Time series of hot-wire data are decomposed into large- and small-scale components, and the impact of the large scale on the amplitude and frequency of the small scales is considered. The amplitude modulation effect is examined by conditionally averaging the small-scale intensity (u_S^2) for various values of the large-scale fluctuation (u_L). It is shown that u_S^2 increases with increasing value of u_L in the near-wall region, whereas, farther away from the wall, u_S^2 decreases with increasing u_L. The rate of increase in small-scale intensity with the strength of the large-scale signal is neither symmetric (about $u_L = 0$) nor linear. The extent of the frequency modulation is examined by counting the number of occurrences of local maxima or minima in the small-scale signal. It is shown that the frequency modulation effect is confined to the near-wall region and its extent diminishes rapidly beyond $y^+ = 100$. A phase lag between the large- and small-scale fluctuations, in terms of amplitude modulation, has also been identified, which is in agreement with previous studies. The phase lag between large- and small-scale fluctuations for frequency modulation is comparable to that of amplitude modulation in the near-wall region. The combined effect of both amplitude and frequency modulation is also examined by computing conditional spectra of the small-scale signal conditioned on the large scales. In the near-wall region, the results indicate that the peak value of pre-multiplied spectra increases with increasing value of u_L, indicating amplitude modulation, while the frequency at which this peak occurs also increases with increasing value of u_L, revealing frequency modulation. The overall trends observed from the conditional spectra are consistent with the results obtained through statistical analyses. Finally, a physical mechanism that can capture most of the above observations is also presented.

Key words: turbulent boundary layers

1. Introduction

It is well established that the outer region of turbulent boundary layers is populated with energetic large-scale structures (Kovasznay, Kibens & Blackwelder

† Email address for correspondence: G.Bharath@soton.ac.uk

1970; Blackwelder & Kovasznay 1972; Brown & Thomas 1977; Wark & Nagib 1991). They are in the form of elongated low- and high-speed regions that meander in the spanwise direction (Ganapathisubramani, Longmire & Marusic 2003; Tomkins & Adrian 2003; Hutchins & Marusic 2007*a*) and have been found in a wide variety of internal flows as well (Kim & Adrian 1999; Del Álamo & Jiménez 2003; Guala, Hommema & Adrian 2006; Monty *et al.* 2007; Bailey *et al.* 2008).

These large-scale structures affect the smaller scales over a range of wall-normal locations. Rao, Narasimha & Narayanan (1971) were perhaps the first to explore this impact when they examined the characteristic value of the burst period in hot-wire signals in the near-wall region and found that these periods scale with the outer variables (boundary-layer thickness, δ, and free stream velocity, U_∞), indicating that bursting might be a large-scale phenomenon in which the large structures in the outer region interact with the near-wall structures. Bandyopadhyay & Hussain (1984) examined the interaction between large and small scales in numerous shear flows, including boundary layers, mixing layers, wakes and jets, by studying short-time correlations between the low- and high-frequency components computed based on hot-wire time-series data. They correlated the low-pass-filtered time-series data with a signal similar to the envelope of the high-frequency component and found significant coupling between scales across all shear flows.

Hutchins & Marusic (2007*b*) examined the impact of large-scale superstructures on near-wall small-scale structure. They found that the largest scales tend to modulate the amplitude of the small-scale fluctuations. Subsequently, Mathis, Hutchins & Marusic (2009) expanded upon these observations and explored this amplitude modulation relationship in greater detail. These authors first split the streamwise velocity into large- and small-scale components via a spectral filter and then used the Hilbert transform to determine the envelope for the small-scale fluctuations. They then correlated the large-scale fluctuations and the low-pass-filtered envelope of the small-scale fluctuations and found that, near the wall, large-scale high-speed regions carry intense superimposed small-scale fluctuations, but this correlation is reversed away from the wall. The location where this reversal takes place appears nominally at the geometric centre of the logarithmic region over a wide range of Reynolds numbers. This amplitude modulation effect has also been captured in conditional analyses performed based on wall shear stress (Hutchins *et al.* 2011). Recently, Marusic, Mathis & Hutchins (2010) and Mathis, Hutchins & Marusic (2011) utilized the information on the correlation between the large-scale fluctuation and the small-scale amplitude and proposed a mathematical model to predict the near-wall turbulence given only large-scale information from the outer boundary-layer region.

Chung & McKeon (2010) analysed large-eddy-simulation (LES) data to study the interaction between the large and small scales and reported findings consistent with Mathis *et al.* (2009). Guala, Metzger & McKeon (2011) used hot-wire data obtained in an atmospheric surface layer to explore these scale interactions. They found similar amplitude modulation effects to the aforementioned studies. They also found that the envelope of the instantaneous dissipation is also correlated with the large-scale fluctuation across various wall-normal locations, indicating that the signature of large scales can be found in the whole wall region and that these scales interact with the near-wall turbulence from the energy-containing eddies down to the dissipative scales. It should be noted that Schlatter & Örlü (2010) indicated that the correlation coefficient between the large-scale signal and the envelope of the small scales is related to the skewness of the raw signal and hence may not be an independent tool to detect or quantify the effect of large-scale amplitude modulation of the small scales.

Nevertheless, the authors indicated that there is indeed an interaction between the large and small scales and therefore there is a need to explore these effects in detail. In fact, in a recent study, Bernardini & Pirozzoli (2011) performed a systematic analysis using two-point amplitude modulation correlation to confirm the top-down influence of large-scale outer events on the inner part of the boundary layer, consistent with the previous work of Hunt & Morrison (2000).

Although these aforementioned studies provide insights into the amplitude modulation effects, the dependence of amplitude modulation on the strength of the large-scale signal is not entirely clear, as the relative contribution of lower- and higher-intensity large-scale fluctuation to amplitude modulation remains unknown. This is primarily because the correlations computed by the aforementioned studies essentially average over all intensities of the large scales. Given that almost all processes in wall-bounded turbulent flows are nonlinear, it can be expected that the strength of the small-scale intensity is strongly linked to the value of large-scale fluctuation. Moreover, none of these previous studies have explored the frequency modulation aspect of the small scales by the large scales. Guala *et al.* (2011) found that dissipation was low when the large-scale fluctuation is negative, while the dissipation was high when the large-scale fluctuation is positive. This suggests that frequency modulation could also play an integral role. However, it must be noted that dissipation is in fact a reflection of both small-scale amplitude and frequency. Therefore, there is a need to explore these effects independently.

In this paper, we explore the role of the strength of large-scale fluctuation in amplitude and frequency modulation of small scales in turbulent boundary layers.

2. Experiments

Experiments were performed in the high-Reynolds-number boundary-layer wind tunnel at the University of Melbourne. This open-return blower wind tunnel has a 27 m long working section, with 2 m $\times$ 1 m cross-sectional area. Further details of the facility are available in Nickels *et al.* (2005, 2007). The pressure gradient is nominally zero, with pressure coefficient (C_p) variation along the entire 27 m length set to within $\pm 0.7\,\%$.

Measurements were performed in the turbulent boundary layer developing over the tunnel floor downstream of the tripped inlet to the working section. The details of the experimental parameters are listed in table 1. The boundary-layer thickness (δ) at the measurement location was obtained by fitting the mean velocity profile to a modified Coles wall/wake formulation. The friction velocity U_τ was calculated from a Clauser fit (Clauser 1956) to mean velocity data using $\kappa = 0.41$ and $A = 5.0$. It should be noted that use of these log law constants has recently come under increasing scrutiny. In this instance, use of $\kappa = 0.384$ and $A = 4.173$, as suggested by Nagib & Chauhan (2008), yields a U_τ that is 0.8 % lower than that obtained with $\kappa = 0.41$ and $A = 5.0$. In any case, the precise value of the estimate for U_τ has no impact on the principal conclusions of this work.

Throughout this paper, x, y and z will be used to denote the streamwise, wall-normal and spanwise axes, with u, v and w denoting the respective fluctuating velocity components. Time is denoted by t and the sample interval by Δt. The superscript $^+$ is used to denote viscous scaling of length (e.g. $y^+ = yU_\tau/\nu$), velocity ($U^+ = U/U_\tau$) and time ($t^+ = tU_\tau^2/\nu$).

The velocity measurements are made using a traversing hot-wire probe. The probe is operated in constant-temperature mode with overheat ratio set to 1.8. Wollaston wires

Re_τ	δ (m)	U_τ (m s^{-1})	U_∞ (m s^{-1})	l^+	Δt^+	No. of points	Domain
14 150	0.326	0.665	20.33	22	0.47	40	$y^+ = 10.64 - y/\delta = 1.38$

TABLE 1. Experimental parameters for hot-wire traverses. All experiments were carried out in the high-Reynolds-number boundary-layer wind tunnel (HRNBLWT) at the University of Melbourne. Further details about these experiments can be found in Hutchins *et al.* (2011).

are soldered across the tips of the probe and etched to give a platinum filament of the desired length. The diameter d and length l of the sensing element were adjusted to give a constant viscous scaled length of $l^+ = 22$ with $l/d \approx 200$, in line with recommendations from Ligrani & Bradshaw (1987) and Hutchins *et al.* (2009). The non-dimensional time interval between samples is $\Delta t^+ \approx 0.47$. A sufficiently long sample length T, approximately 18 950 boundary-layer turnover times (TU_∞/δ, where U_∞ is the free stream velocity), was used to converge the energy contained in the largest scales. Further details of the experimental set-up and the data can be found in Hutchins *et al.* (2011).

3. Methods

In this paper, we focus on examining the interaction between the large and small scales of the boundary layer. Therefore, for brevity, we have not included detailed information on the unconditional flow statistics such as mean profiles. These mean and root-mean-square (r.m.s.) profiles can be found in Hutchins *et al.* (2011).

3.1. *Filter scheme*

The goal is to examine the amplitude and frequency modulation effects of the large scales on the small scales in wall turbulence. Therefore, a suitable filtering technique is necessary to separate the large and the small scales. The fluctuating streamwise velocity (u) across the boundary layer is decomposed into large- and small-scale fluctuations using a spectral filter. The streamwise velocity is low-pass-filtered to obtain the large-scale fluctuation (u_L) and the small-scale signal (u_S) is computed by subtracting this large-scale velocity fluctuation from the raw streamwise velocity fluctuation, i.e. $u_S = u - u_L$. The details of the filter are given in table 2. It must be noted that the small scales in themselves includes a broad range of scales ranging from the near-wall streaks down to the Kolmogorov scales. Although we can separate the small scales further with subsequent filtering, the aim of this study is to identify the overall relationship between large-scale structures and the small scales that are an order of magnitude smaller than the large scales. Therefore, our filter is chosen to ensure that we clearly separate the large scales from the near-wall small scales. This filtering procedure is identical to the methodology followed in Mathis *et al.* (2009).

Previous studies have also used a box filter to separate the large- and small-scale fluctuations (Bandyopadhyay & Hussain 1984; Chung & McKeon 2010; Guala *et al.* 2011). A box filter does not provide a sharp cutoff point between the large and small scales and therefore could lead to contamination in the energy content of the large and the small scales. Therefore, we only present the analyses carried out using the spectral filter. However, we found that the results presented in this paper are qualitatively similar regardless of the filtering technique used.

Fluctuation	Designation	Time scales captured
u	Streamwise velocity fluctuation	$\lambda_t^+ \geqslant 0.47$
u_L	Large-scale fluctuation	$\lambda_t U_\infty/\delta > 2$
$u_S = u - u_L$	Small-scale fluctuation	$\lambda_t^+ \geqslant 0.47$ and $\lambda_t U_\infty/\delta \leqslant 2$

TABLE 2. Filter parameters for scale decomposition.

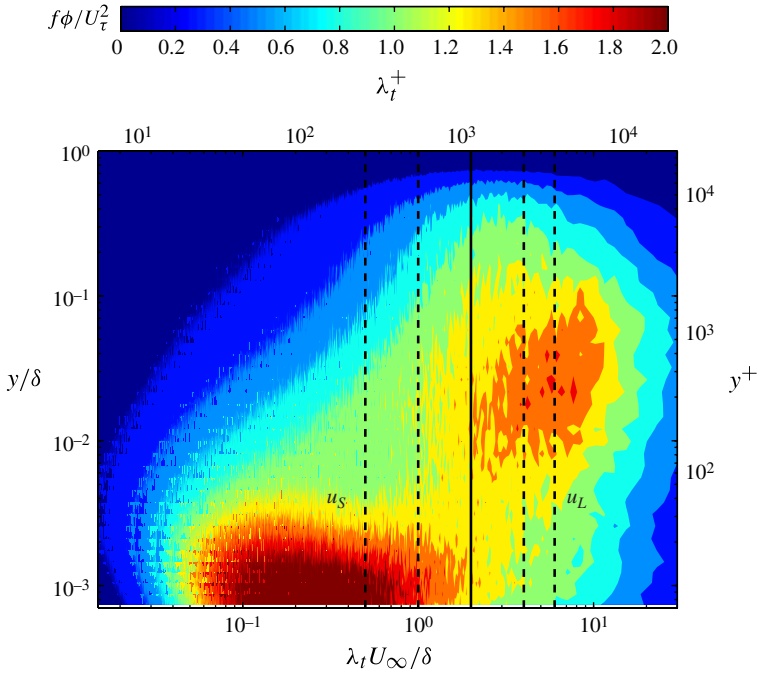

FIGURE 1. Pre-multiplied energy spectra of the streamwise velocity fluctuations, $f\phi_{uu}/U_\tau^2$, as a function of wall-normal location and time scale. The wall-normal location and the time scale are normalized by both outer scales (U_∞ and δ) and inner scales (U_τ and ν). The vertical lines at $\lambda_t U_\infty/\delta = 0.5,\ 1,\ 2,\ 4$ and 6 show the different filter time scales used to separate the large scales from the small scales.

The filter length is important, as this choice enables us to separate the large scales from the small scales. Consider the pre-multiplied energy spectrogram depicted in figure 1. This spectrogram shows the energy content of the fluctuations as a function of temporal scales and wall-normal location. The vertical lines at $\lambda_t U_\infty/\delta = 0.5,\ 1,\ 2,\ 4$ and 6 show a selection of different filter lengths that could be used to separate the large scales and the small scales. The energy content to the left of any of these vertical lines is attributed to small-scale fluctuations, and the energy content to the right of these lines is the contribution from the large-scale structures. The small-scale fluctuations account for the majority of the near-wall peak and their energy content decays throughout the logarithmic region. The large-scale component, on its own, makes a significantly lower contribution compared to the small-scale component in the near-wall region. However, it should be noted that large scales do make a contribution to the turbulent fluctuations near the wall, reinforcing the fact

that large-scale structures maintain a footprint in the near-wall region. Farther away from the wall, the large scales make an increasingly large contribution to the turbulent fluctuations. It must be noted that, in this study, we present all our results in the time/frequency domain. Converting time-domain data into spatial-domain data requires a convection velocity and, since it is well established that this convection velocity varies not just with scales but also with wall-normal location (Dennis & Nickels 2008; Del Álamo & Jiménez 2009; Chung & McKeon 2010), we refrain from converting the time-domain data into the spatial domain.

Figure 1 also indicates that a filter time scale of $\lambda_t U_\infty/\delta = 2$ (depicted using the solid vertical line) appears to clearly demarcate the high-energy lobe in the near-wall region (with peak at $\lambda_t U_\infty/\delta \approx 0.2$ or $\lambda_t^+ \approx 100$) from the high-energy lobe in the outer region (with peak at around $\lambda_t U_\infty/\delta \approx 5.5$). All other filter scales infringe upon the near-wall lobe (filters with length $\lambda_t U_\infty/\delta = 0.5$ and 1) or extend into the lobe in the outer region ($\lambda_t U_\infty/\delta = 4$ and 6). Therefore, unless otherwise specified, the results presented in this paper are obtained using a filter length of $\lambda_t U_\infty/\delta = 2$ to distinguish between the large and small scales. The quantitative effects of varying the filter length are investigated in appendix B. However, it should be noted here that using any of the filters described in figure 1 makes remarkably little difference to the overall results and conclusions of this study. It is also worth noting that there is very little difference in the filter length if it is calculated based on the local mean velocity rather than on the free stream velocity. The filter scale based on local mean (as done by Mathis *et al.* 2009) would be in the range $0.8 \leqslant \lambda_t U_\infty/\delta \leqslant 2$, since the local mean across all wall-normal locations is in the range $0.4 \leqslant U(y)/U_\infty \leqslant 1$ (see Hutchins *et al.* 2011).

Figure 2(*a*) shows a comparison between the large-scale fluctuations and small-scale velocity fluctuations at $y^+ = 15$. The figure clearly indicates that the amplitude of the small-scale fluctuations depends on the sign of the large-scale fluctuations. Two examples, one for negative values of u_L and the other for positive values of u_L, are depicted in figures 2(*b*) and 2(*c*), respectively. These two representative events are marked with rectangles in figure 2(*a*). For negative values of large-scale fluctuations, the amplitude of small-scale fluctuations appears diminished. On the contrary, the amplitude of small scales is higher for positive fluctuations of the large scales. This suggests that the large-scale fluctuations tend to modulate the amplitude of the small scales in the near-wall region. In addition to the amplitude modulation effects, figures 2(*b*) and 2(*c*) indicate that the frequency of the small-scale fluctuations is also modulated. It can be visually confirmed that the frequency of small-scale fluctuations for negative values of u_L is lower compared to the frequency of small-scale fluctuations for positive values of u_L. This frequency modulation effect has not been explored before. In the following sections, we will explore both the amplitude and frequency modulation effects over a range of wall-normal locations in a high-Reynolds-number turbulent boundary layer.

4. Amplitude modulation

As mentioned previously, Mathis *et al.* (2009) found a high degree of correlation between the envelope of the small-scale signal and the large-scale signal near the wall. Chung & McKeon (2010) and Guala *et al.* (2011) used LES data from a channel flow simulation and atmospheric surface layer data, respectively, in liaison with a filtering technique identical to the one used in the current study, and also found a similar trend in the relationship between large and small scales. Although this provides insights into the amplitude modulation effects, the dependence of amplitude modulation on

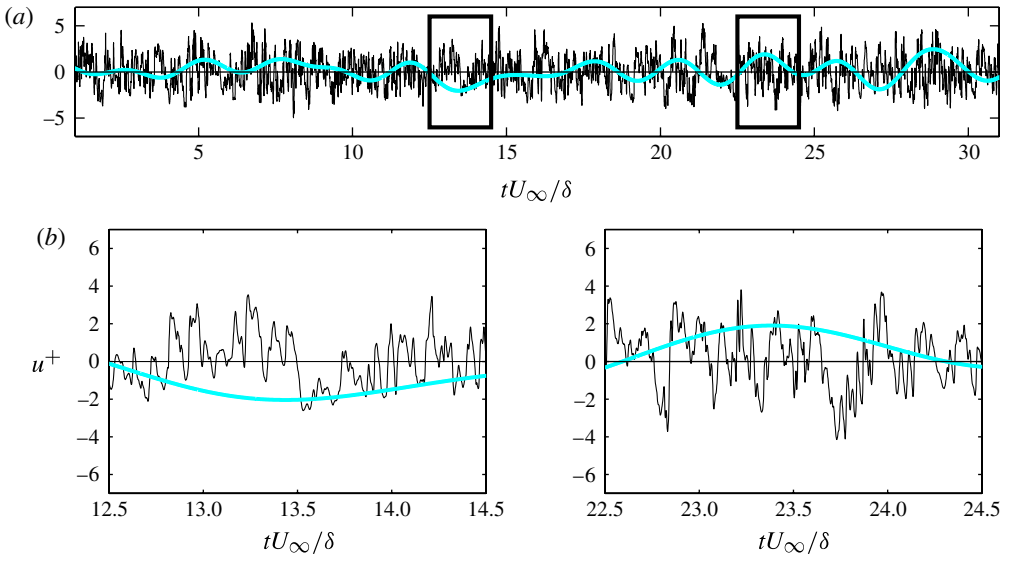

FIGURE 2. (*a*) Instantaneous example of amplitude and frequency modulation of the small scales by the large scales at $y^+ = 15$ ($y/\delta = 0.001$). (*b*) A close-up view of the low- and high-speed large-scale fluctuations (marked with rectangles) in figure 2(*a*). The grey (cyan coloured) thicker lines show the large-scale fluctuation (u_L^+) and the black lines the corresponding small-scale fluctuation (u_S^+). The large scale and the small scales are computed based on a filter time scale of $\lambda_t U_\infty/\delta = 2$.

the strength of the large-scale signal is not very clear. This link can be explored by computing the small-scale amplitude conditioned on the value of large-scale intensity.

Figure 3 shows a schematic representation of the procedure followed to isolate the effects of large scales on the amplitude of the small scales. As shown in the figure, the aim is to compute the conditional amplitude of the small scales conditioned on the intensity of the large-scale fluctuation. The step-by-step procedure used to compute this conditional small-scale amplitude is as follows.

(i) The velocity fluctuation (u) is separated into large-scale (u_L) and small-scale (u_S) fluctuations by using a spectral filter of length $\lambda_t U_\infty/\delta = 2$.

(ii) Equally spaced bins with a spacing of 0.2 ranging from $u_L^+ = -6$ to $u_L^+ = 6$ are created for the large-scale fluctuations. The bin spacing of 0.2 is chosen as a balance between bin size and the number of samples within each bin. Bins with smaller size encountered problems with statistical convergence, as fewer than 100 samples were detected for bins with smaller sizes.

(iii) The time series of both the large- and small-scale fluctuations are divided into individual segments of length $\lambda_t U_\infty/\delta = 2$ (which is the filter time scale that delineates the large scale from the small scales). These individual segments are used to analyse the relationship between large- and small-scale fluctuations.

(iv) The representative value of the large-scale fluctuation (u_L^+) in a segment is chosen as the value at the centre of an individual segment.

(v) The variance of the small-scale signal over the same segment (u_S^{2+}) is also computed, and this small-scale variance is the amplitude of the small scales conditioned on the strength of the representative large-scale signal, $u_S^{2+}|_{u_L^+}$.

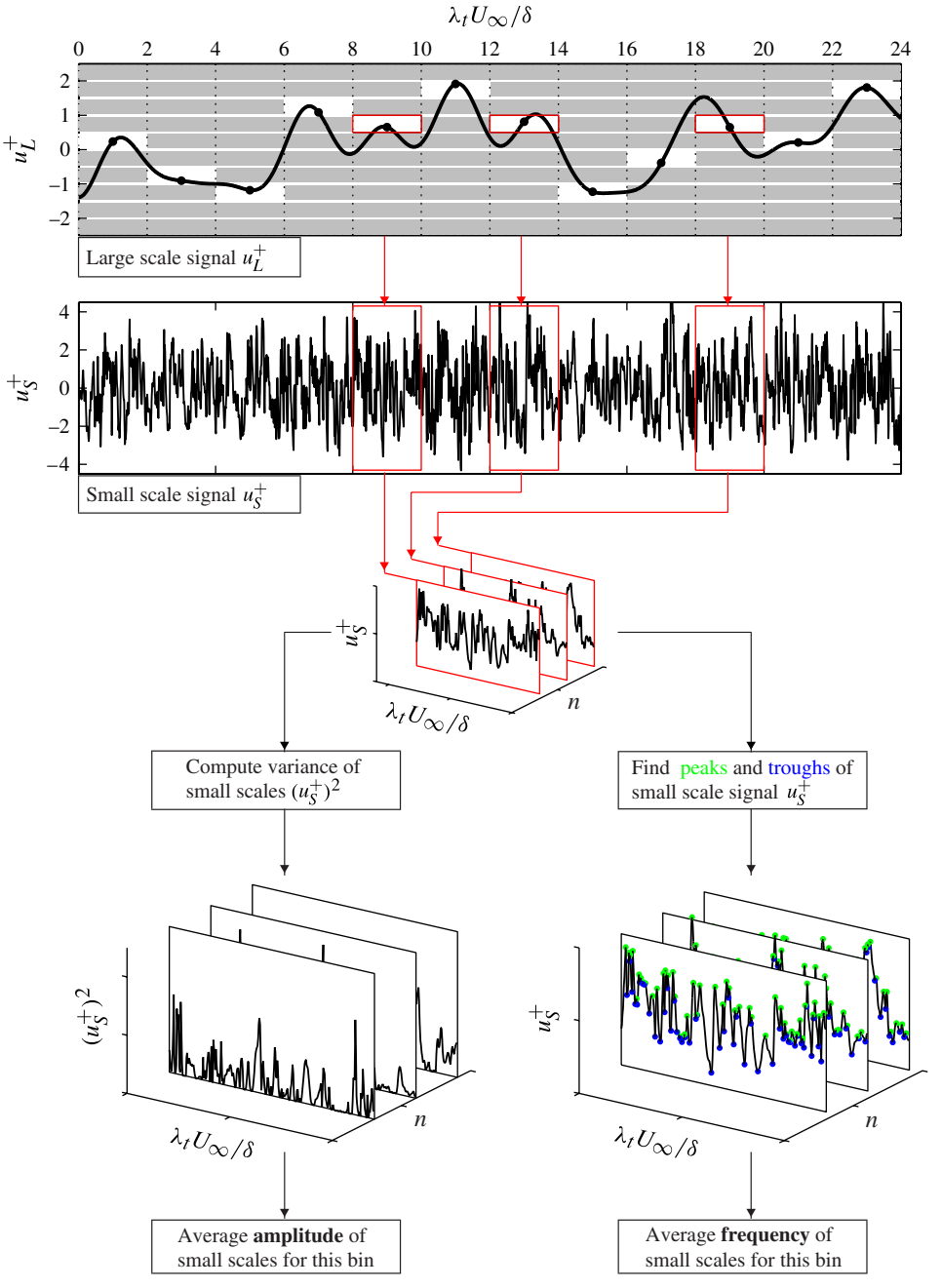

FIGURE 3. Procedure followed to isolate the amplitude and frequency modulation effects of the large scales on the small scales at a given wall-normal location. The schematic shows the procedure followed to calculate the amplitude and frequency of the small scales for a given value of the large-scale fluctuation. This procedure is repeated across all wall-normal locations.

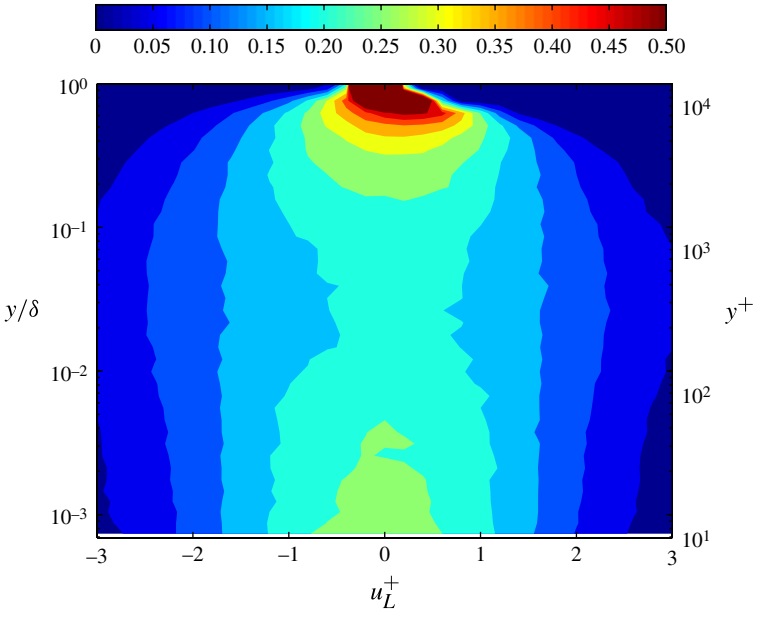

FIGURE 4. Probability density function of the large-scale fluctuation across all wall-normal locations.

(vi) Steps (iv)–(v) are repeated for all segments and across all wall-normal locations.

(vii) The number of occurrences of the representative fluctuation (u_L^+) within each bin is also calculated across all wall-normal locations, $N[u_L^+(y)]$.

(viii) A mean small-scale variance for each bin of the large-scale fluctuation is calculated at all wall-normal locations,

$$\langle u_S^{2+}(u_L^+, y)\rangle = \frac{\sum u_S^{2+}(y)|_{u_L^+(y)}}{N[u_L^+(y)]}. \tag{4.1}$$

This represents the amplitude of the small scales conditioned on the value of large-scale fluctuation.

Prior to exploring these conditional variances, it is important to examine the distribution of u_L^+. Figure 4 shows the probability density function (p.d.f.) of u_L^+ over all wall-normal locations. This probability distribution is computed based on the number of occurrences of u_L^+ within a given threshold:

$$\text{p.d.f.}[u_L^+(y)] = \frac{N[u_L^+(y)]}{\int N[u_L^+(y)]\,\mathrm{d}u_L^+}. \tag{4.2}$$

In order to ensure statistical convergence, we only utilize and present data if the number of samples in any u_L^+ bin exceeds a minimum value (in this case, this value is set to 100 samples per bin). The figure indicates that the p.d.f. is effectively symmetric about $u_L^+ = 0$ across all wall-normal locations. The p.d.f. is relatively narrow in the near-wall region consistent with the fact that the near-wall fluctuations are dominated by the small scales. This p.d.f. is broader in the log region where the large scales

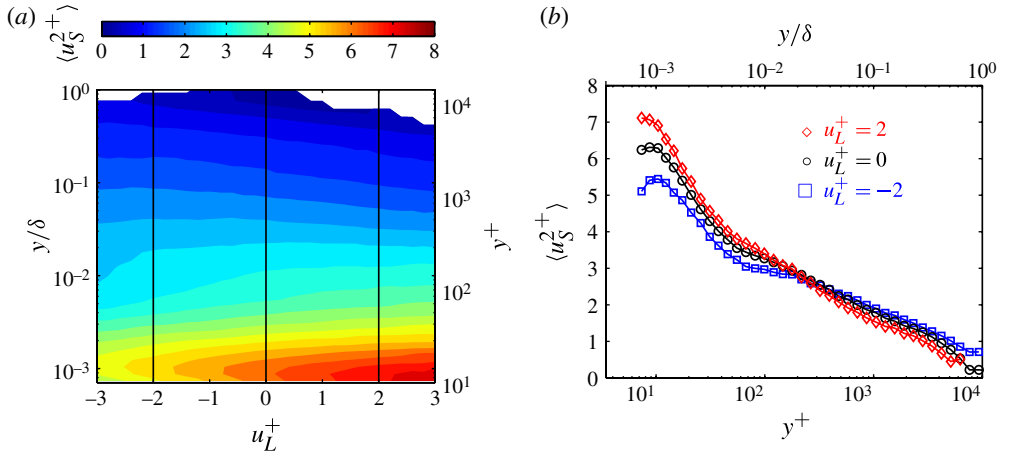

FIGURE 5. (*a*) Small-scale variance as a function of large-scale fluctuation and wall-normal location, $\langle u_S^{2+}(u_L^+, y)\rangle$. (*b*) Small-scale variance as a function of wall-normal location for $u_L^+ = -2$, 0 and 2. The large- and small-scale fluctuations are based on a filter time scale of $\lambda_t U_\infty/\delta = 2$.

dominate the velocity fluctuations and becomes narrow again in the outer wake region where the flow is intermittent.

Given this distribution in the large scales, the amplitude modulation of the small scales by the large scales can now be explored in detail. Figure 5(*a*) shows $\langle u_S^{2+}\rangle$ as a function of u_L^+ and wall-normal location. It is clear from this figure that the amplitude of the small scales is indeed modulated by the large-scale fluctuation over a range of wall-normal locations. In the near-wall region, the amplitude of the small scales is markedly lower for negative values of u_L^+ compared to the positive values of u_L^+.

The amplitude modulation effect can be further explored by examining the small-scale variance in three representative bins of u_L^+. Figure 5(*b*) shows the wall-normal variation of small-scale variance for $u_L^+ = -2$, 0 and 2. Near the wall, the small-scale fluctuations for $u_L^+ = 2$ possess higher intensity than the small-scale fluctuations for $u_L^+ = -2$. This suggests that the near-wall small-scale fluctuations are strengthened in the presence of a large-scale high-speed event. It must be noted that the differences observed in figure 5(*b*) are significantly larger than the statistical uncertainty, which is less than 1 % of the value (this is also true for the frequency modulation results presented in subsequent sections). Figure 5(*b*) also shows that $\langle u_S^{2+}\rangle$ for $u_L^+ = -2$ becomes higher than $\langle u_S^{2+}\rangle$ for $u_L^+ = 2$ at $y/\delta \approx 0.03$ ($y^+ \approx 400$) and remains higher throughout the outer log region. This cross-over point is consistent with the cross-over location in the amplitude modulation coefficient found by Mathis *et al.* (2009), where $y_c^+ \approx 3.9\sqrt{Re_\tau} \approx 460$. This indicates that, away from the wall, the presence of a high-speed large-scale event leads to diminished small-scale turbulence activity. Conversely, a low-speed large-scale event is associated with intense small-scale fluctuations away from the wall. The trends exhibited by these profiles are consistent with the conditional small-scale variance (conditioned on the presence of large-scale skin-friction fluctuation) presented in Hutchins *et al.* (2011). It is also consistent with the profiles in Guala *et al.* (2011), who computed small-scale variance conditioned on $u_L^+ > 0$ and $u_L^+ < 0$.

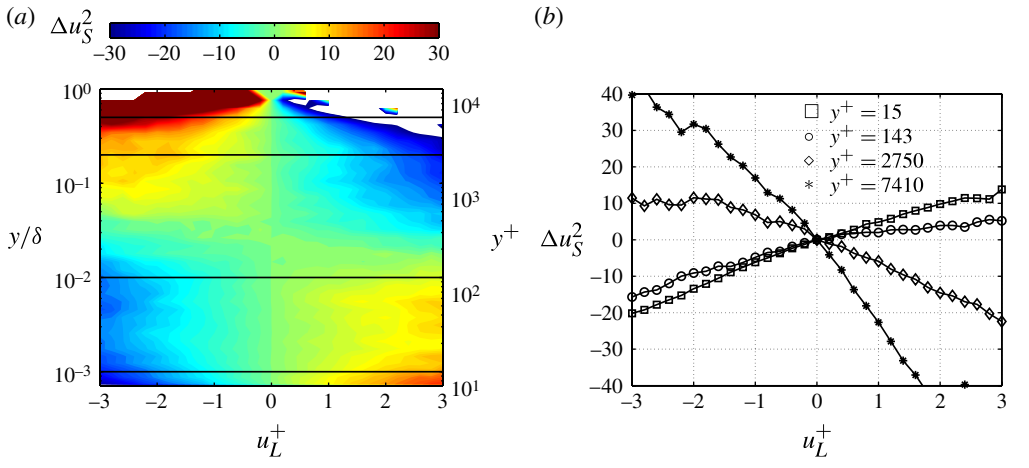

FIGURE 6. (*a*) Plot of Δu_S^2 as a function of wall-normal location and u_L^+. (*b*) Plot of Δu_S^2 at four wall-normal locations, $y^+ = 15$, 143, 2750 and 7410. The large- and small-scale fluctuations are based on a filter time scale of $\lambda_t U_\infty/\delta = 2$.

The small-scale variance for $u_L^+ = 0$ depicts the behaviour of the small-scale amplitude when the concurrent large scales are weak. Therefore, we can define an amplitude difference parameter as the relative difference between $\langle u_S^{2+}(u_L^+)\rangle$ and $\langle u_S^{2+}(u_L^+ = 0)\rangle$,

$$\Delta u_S^2(u_L^+, y) = \frac{\langle u_S^{2+}(u_L^+, y)\rangle - \langle u_S^{2+}(u_L^+ = 0, y)\rangle}{\langle u_S^{2+}(u_L^+ = 0, y)\rangle} \times 100, \tag{4.3}$$

where a positive percentage difference indicates amplitude amplification relative to $u_L^+ = 0$ and a negative difference should reveal amplitude attenuation. This $u_L^+ = 0$ bin is subsequently referred to in this paper as the unmodulated information because the strength of the carrier signal (i.e. u_L) is in fact zero. It must be noted that the small-scale signal for the $u_L = 0$ bin is only 'locally' unmodulated at a given wall-normal location. The filtering and binning process does not account for non-local modulation effects where the small scales at a given wall-normal location are affected by the large-scale fluctuations above or below the given wall-normal location.

Figure 6(*a*) shows contours of Δu_S^2 as a function of u_L^+ and wall-normal location. Amplitude modulation (both amplification and attenuation) of over 30 % is realized in the near-wall as well as outer regions. The fact that the contours are not symmetric about $u_L^+ = 0$ indicates that the relative amplitude attenuation for negative values of large-scale fluctuation is higher than the amplitude amplification for positive values of u_L^+. This feature can be further explored through a closer inspection of the percentage difference at different wall-normal locations.

Figure 6(*b*) shows the Δu_S^2 profiles at four wall-normal locations, $y^+ = 15$, 143, 2750 and 7410. The four locations are marked with horizontal lines in figure 6(*a*). These profiles at all four locations emphasize the extent of symmetry (or lack thereof) in amplitude modulation. In the near-wall region (i.e. $y^+ = 15$), the difference reaches a values of -20 % for $u_L^+ = -2$; however, it only reaches $+10$ % for $u_L^+ = 2$. Similar asymmetric trends are observed in all other wall-normal locations. In addition to the asymmetry, figure 6(*b*) also shows that the modulation effect is not linear. This is

consistent with the results obtained by Mathis *et al.* (2009), where the correlation between the large-scale signal and the filtered envelope of the small scales was never one. This is also consistent with the correlation between the large and small scales found in other studies (Bandyopadhyay & Hussain 1984; Chung & McKeon 2010; Guala *et al.* 2011). It must be noted that a correlation coefficient is a measure of the strength of linear dependence between two parameters. A correlation value of one implies that a linear equation perfectly describes the relationship between the two parameters. Deviation from one in the correlation coefficient reveals the existence of a nonlinear relationship between the two parameters (if there is any relationship at all). Therefore, the fact that the correlation between the large-scale signal and the filtered envelope of the small scales was never equal to one (in Mathis *et al.* 2009; Chung & McKeon 2010; Guala *et al.* 2011) is consistent with the current observations. The correlation between the large-scale signal and the envelope of the small-scale amplitude in Mathis *et al.* (2009) was as high as 0.7 in the near-wall region. This indicates that the relationship between the large scales and the amplitude of the small scales is probably dominated by linear dependence.

5. Frequency modulation

Figure 2(*b*) also reveals the presence of frequency modulation effects. It can be seen that the frequency of small-scale fluctuations for negative large-scale fluctuation is attenuated (together with the amplitude), with positive and negative excursions in the small-scale fluctuation occurring at a relatively low frequency. Conversely, the frequency of small-scale fluctuations for positive value of u_L^+ is relatively high, with positive and negative excursions occurring in rapid succession at higher frequencies. Perhaps, this effect was noted by Rao *et al.* (1971), who found that the band-pass-filtered bursting frequency in the near-wall region increased with their amplitude 'descriptor setting'. However, since the authors did not differentiate between positive and negative excursions, they were unable to isolate the effects of this frequency modulation.

The frequency characteristics of the small-scale instantaneous signal in figure 2 is also consistent with Guala *et al.* (2011), who computed conditional dissipation as a function of large-scale fluctuation and wall-normal location. They found that the dissipation levels were indeed lower for $u_L < 0$ and higher for $u_L > 0$. It must be noted that dissipation has both amplitude and frequency effects embedded in it. A high value of dissipation, which occurs as a result of the presence of high gradients, can occur due to either a large amplitude of fluctuation or the presence of higher frequencies. Consequently, this conditional dissipation presented in Guala *et al.* (2011) includes both frequency and amplitude modulation effects. Since we have already explored the effects of amplitude modulation, we need a new metric to quantify the impact of frequency modulation that is independent of amplitude modulation effects.

One way to determine a characteristic frequency of the small scales is to examine the zero-crossing frequency in the small-scale fluctuation. This method has been applied previously by various researchers to examine the time and length scale distributions of various flows, including turbulent boundary layers (Sreenivasan, Prabhu & Narasimha 1983; Kailashnath & Sreenivasan 1993). However, as pointed out by Sreenivasan *et al.* (1983) and Sreenivasan (1985), various factors, including the dynamic range of the signal, the value of the thresholds used, the filter frequency and noise contamination, have a strong bearing on the results obtained. Moreover, the zero-crossing frequency will exclude frequency information that is not associated with

zero crossings. Therefore, zero-crossing frequency may not be ideal to determine the characteristic frequency of the small scales. Alternative time-domain cycle counting procedures such as peak counting as well as peak–valley counting have also been proposed to examine the frequency content (see e.g. Rychlik 1993). These methods have their own set of drawbacks, as they tend to bias the signal towards higher frequencies, and previous work has examined the relative merit of employing these technique to broadband and bimodal signals (Repetto 2005). In the current study, we propose to follow a method that is based on the peak–valley counting (PVC) procedure to determine the relative extent to which the high frequencies (i.e. the frequency of the small scales) depend on the strength of the large-scale fluctuation. The drawbacks of using a method based on the PVC procedure (i.e. possible bias towards high frequencies) are not relevant to our analysis since the small-scale signal is already high-pass-filtered to include only high-frequency content. In our method, we count the number of local maxima and minima over a given sample length and use it to calculate a representative frequency for the same sample (by dividing the number of local maxima or minima by the sample length). For a constant sample length (which it is, in the current study, see below), the higher the number of local maxima and minima per unit length, the higher the representative frequency of the signal.

Figure 3 showed a flowchart of the procedure followed to isolate the effects of large scales on the small scales. The step-by-step procedure to compute the frequency of occurrence of local maxima and minima (f_m) in the small-scale signal per unit length of the large scale is given below. It must be noted that the first three steps of the procedure are identical to the one followed in § 4. For the sake of completeness, we document the entire procedure here.

(i) The velocity fluctuation (u) is separated into large-scale (u_L) and small-scale (u_S) fluctuations by using a spectral filter of length $\lambda_t U_\infty/\delta = 2$.

(ii) Equally spaced bins with a spacing of 0.2 ranging from $u_L^+ = -6$ to $u_L^+ = 6$ are created for the large-scale fluctuations.

(iii) The time series of both the large- and small-scale fluctuations are divided into individual segments of length $\lambda_t U_\infty/\delta = 2$ (which is the filter time scale that delineates the large scale from the small scales). These individual segments are used to analyse the relationship between large- and small-scale fluctuations.

(iv) The representative value of the large-scale fluctuation (u_L^+) in a segment is chosen as the value at the centre of an individual segment.

(v) The number of local maxima or minima (i.e. $\partial u_S^+/\partial t = 0$) in the small-scale signal over the same segment is computed (N_m).

(vi) A representative frequency of occurrence of local maxima or minima per unit length is computed as $f_m = N_m/2\lambda_t$, and this value is assigned to the bin corresponding to the value of large-scale fluctuation. The frequency is in fact the spacing between two successive maxima or minima. Since, we count both maxima and minima in our procedure, the factor 2 is introduced in the denominator. This frequency represents the frequency of the small scales conditioned on the strength of the large-scale fluctuation, $f_m|_{u_L^+}$.

(vii) Steps (iv) and (vi) are repeated for all segments and across all wall-normal locations.

(viii) The number of occurrences of the representative fluctuation (u_L^+) within each bin is also calculated across all wall-normal locations, $N[u_L^+(y)]$.

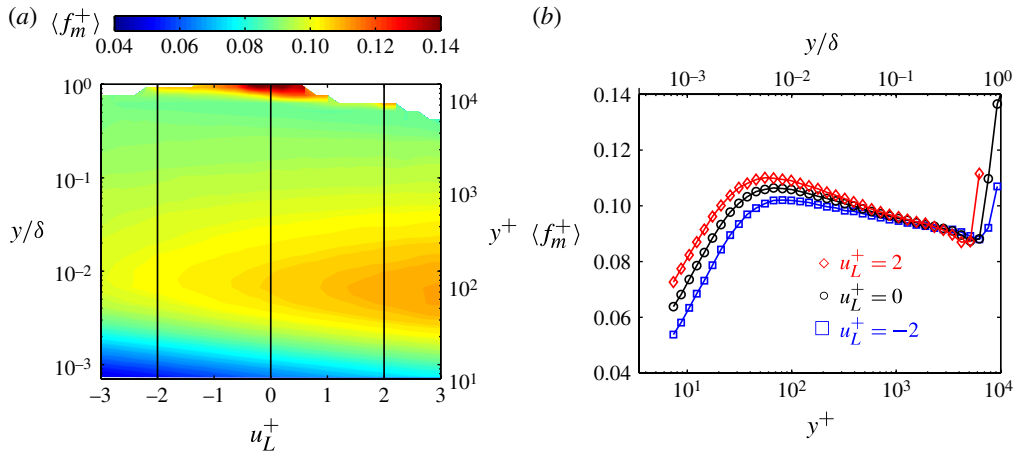

FIGURE 7. (*a*) Plot of $\langle f_m^+ \rangle$ as a function of u_L^+ and y/δ. (*b*) Plot of $\langle f_m^+ \rangle$ as a function of wall-normal location at $u_L^+ = -2$, 0 and 2. The large- and small-scale fluctuations are based on a filter time scale of $\lambda_t U_\infty/\delta = 2$.

(ix) A mean representative frequency of the small scales for every bin of the large-scale fluctuation is calculated at all wall-normal locations,

$$\langle f_m(u_L^+, y)\rangle = \frac{\sum f_m(y)|_{u_L^+(y)}}{N[u_L^+(y)]}. \tag{5.1}$$

This represents a characteristic frequency of the small scales conditioned on the value of large-scale fluctuation.

The frequency of occurrence of local maxima or minima per unit length provides a characteristic frequency for the small-scale fluctuations. A lower value of f_m indicates lower values of N_m, which in turn suggests the presence of lower frequencies in the small scales, whereas a large value of f_m shows higher frequencies (i.e. smaller time scales). Figure 7(*a*) shows f_m as a function of u_L^+ and wall-normal location. The figure indicates that the characteristic frequency is lower in the near-wall region and increases with increasing wall-normal location across all values of u_L^+ up to $y^+ = 100$. This is in contrast with amplitude modulation where the maximum modulation decreases monotonically with increasing wall-normal distance.

The rate of increase in frequency modulation with increasing wall-normal location depends on the value of u_L^+. This varying rate of increase is clearly seen from the fact the contours are inclined with respect to the u_L^+ axis. This increasing frequency with wall-normal location can be examined in detail by looking at the wall-normal variation of $\langle f_m \rangle$ at three representative bins of u_L^+. Figure 7(*b*) shows the variation of f_m with wall-normal location for $u_L^+ = -2$, 0 and 2. The figure shows that, in the near-wall region, the characteristic frequency is consistently higher with increasing value of u_L^+. It can also be seen that f_m for all three bins collapses in the outer region, for $y/\delta > 0.1$ ($y^+ > 1450$). In the outer wake region there is no difference in the characteristic frequency for different values of u_L^+.

As is the case with amplitude modulation, the characteristic frequency for $u_L^+ = 0$ should provide the unmodulated small-scale frequency. Again, it must be noted that the small-scale signal for the $u_L = 0$ bin is only 'locally' unmodulated. The filtering

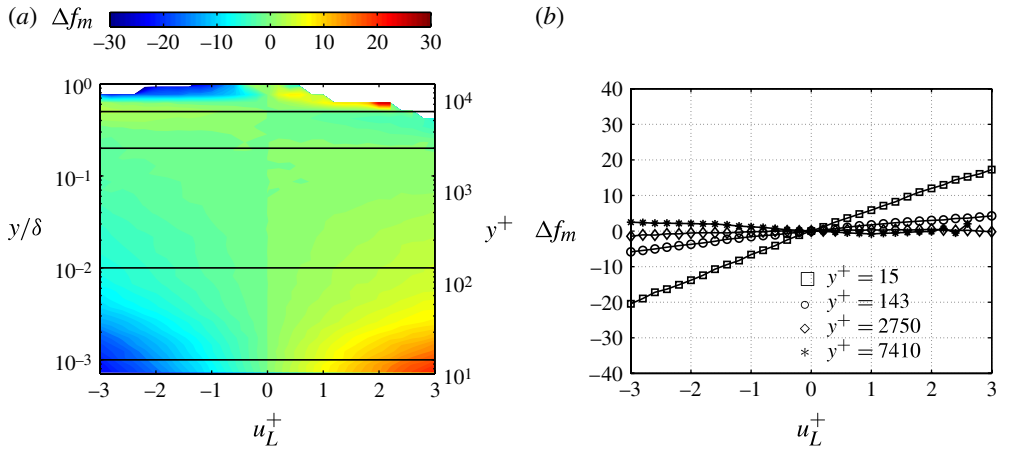

FIGURE 8. (*a*) The percentage difference in $\langle f_m^+ \rangle$ computed relative to $u_L^+ = 0$. (*b*) Plot of Δf_m at four different wall-normal locations. The large- and small-scale fluctuations are based on a filter time scale of $\lambda_t U_\infty/\delta = 2$.

and binning process does not account for non-local modulation effects where the small scales at a given wall-normal location are affected by the large-scale fluctuations above or below the given wall-normal location.

The relative difference between $f_m(u_L^+)$ and $f_m(u_L^+ = 0)$ should clearly show the effects of frequency modulation. Therefore, we define a characteristic frequency difference parameter as

$$\Delta f_m(u_L^+, y) = \frac{\langle f_m(u_L^+, y)\rangle - \langle f_m(u_L^+ = 0, y)\rangle}{\langle f_m(u_L^+ = 0, y)\rangle} \times 100. \tag{5.2}$$

A positive percentage difference indicates an increase in frequency relative to the 'unmodulated' value, and a negative difference should reveal a decrease in frequency of fluctuations.

Figure 8(*a*) shows contours of Δf_m as a function of u_L^+ and wall-normal location. Frequency modulation (both amplification and attenuation) of over 30 % is realized in the near-wall region; however, the extent of frequency modulation diminishes in the outer region and beyond. The contours appear to be symmetric in the near-wall region (up to $y^+ \approx 100$), suggesting an equal and opposite effect for positive and negative values of u_L^+. This is perhaps understandable if we interpret negative values of u_L^+ as essentially realizations of lower Reynolds numbers compared to those with positive values of u_L^+. This difference in 'local' Reynolds numbers should result in 'lower' frequencies in small scales for $u_L^+ < 0$. This feature can be further explored through a closer inspection of the percentage difference at different wall-normal locations.

Figure 8(*b*) shows the variation of Δf_m with u_L^+ for four wall-normal locations. Near the wall (at $y^+ = 15$), the characteristic frequency increases with increasing large-scale fluctuation. In the log region ($y^+ = 143$), the frequency still increases with increasing value of u_L^+; however, the rate of increase (as determined by the slope of the curve) is lower at this location compared to the rate of increase at $y^+ = 15$. Farther away from the wall at $y/\delta = 0.19$, the characteristic frequency appears to be constant across the entire range of u_L^+. This suggests that the frequency modulation effect is highest in the near-wall region and this effect decreases with increasing wall-normal distance. Towards the edge of the boundary layer, frequency modulation

effects reappear; however, owing to lack of statistical convergence in the data, we are unable to further explore this in detail. Presumably, this effect towards the edge of the boundary layer is an artefact of intermittency where irrotational flow from the free stream penetrates the boundary layer due to entrainment.

The above observations on frequency modulation can be interpreted as follows. If we consider positive large-scale fluctuations, they are observed to increase the frequency of the small scales. This increase in small-scale frequency can be viewed as follows: either the number of small-scale structures increases, or the small scales are convected faster past our stationary probe by the positive large-scale fluctuations. In fact, it is likely that we have a combination of these two scenarios, but the present measurements cannot distinguish between them. Therefore, frequency modulation should be viewed as a combination of both augmented small-scale activity and convection of these small scales by the large-scale motions.

6. Phase information in amplitude and frequency modulation

It must be noted that all the analysis performed thus far does not account for any phase difference between large and small scales. A phase difference between large and small scales was first observed by Bandyopadhyay & Hussain (1984) and more recently by Chung & McKeon (2010), Guala *et al.* (2011) and Hutchins *et al.* (2011) for amplitude modulation. All these studies found that this phase difference increases with increasing distance from the wall. In this section, we examine this phase difference in detail and attempt to explain its dependence on the strength of the large-scale fluctuation.

The phase difference (or time lag/lead) between the amplitude or frequency of the small scales and the strength of the large-scale fluctuations can be easily computed by conditionally averaging the amplitude and frequency of the small scales at various time separations from a given large-scale fluctuation. These conditional averages can be computed using the same procedure as outlined in the previous sections, but the procedure now includes a temporal shift as well.

The amplitude and the frequency of the small scales can be computed as

$$\langle u_S^{2+}(u_L^+, y, \tau)\rangle = \frac{\sum u_S^{2+}(y, t+\tau)|_{u_L^+(y,t)}}{N[u_L^+(y)]}, \tag{6.1}$$

$$\langle f_m^+(u_L^+, y, \tau)\rangle = \frac{\sum f_m^+(y, t+\tau)|_{u_L^+(y,t)}}{N[u_L^+(y)]}, \tag{6.2}$$

where N is the number of occurrences of u_L^+ within a certain bin and τ is the time shift between the representative large-scale fluctuation at time t (which is located at the centre of a segment of length $\lambda_t U_\infty/\delta = 2$) and the small-scale amplitude or frequency (which is also calculated over a segment of length $\lambda_t U_\infty/\delta = 2$ and its temporal location is the centre of that segment). In §§ 4 and 5, we presented the data for $\tau = 0$, where the representative large-scale fluctuation and the small-scale amplitude or frequency were computed using the same segment of data. In this section we will present the amplitude and frequency of the small scales as a function of wall-normal location, the strength of large-scale fluctuation and time delay. This will allow us to explore the phase difference between the large and small scales as a function of the strength of the large-scale fluctuation.

Just as in previous sections, we define an amplitude or frequency difference parameter as the relative difference between the amplitude or frequency of the small

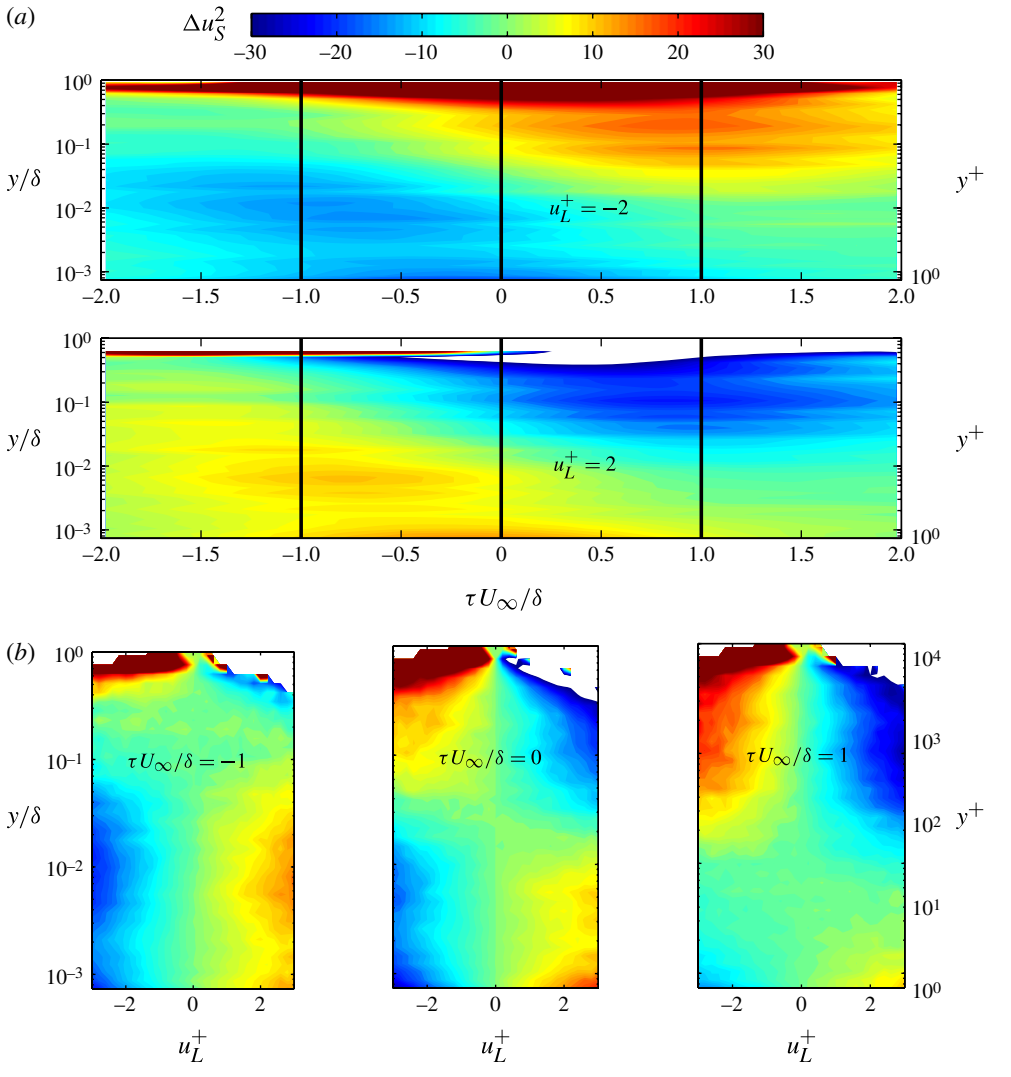

FIGURE 9. (*a*) The top plot shows Δu_S^2 as a function of phase difference (τ) and wall-normal location (y) for $u_L^+ = -2$; and the bottom plot shows $\Delta u_S^{2+}(\tau, y)$ for $u_L^+ = 2$. (*b*) The three plots show Δu_S^2 as a function of u_L^+ and wall-normal location at three different phases, $\tau U_\infty/\delta = -1$, 0 and 1.

scales for a given u_L^+ and time delay τ and the amplitude or frequency at $u_L^+ = 0$ at $\tau = 0$:

$$\Delta u_S^2(u_L^+, y, \tau) = \frac{\langle u_S^{2+}(u_L^+, y, \tau)\rangle - \langle u_S^{2+}(u_L^+ = 0, y, \tau = 0)\rangle}{\langle u_S^{2+}(u_L^+ = 0, y, \tau = 0)\rangle} \times 100, \tag{6.3}$$

$$\Delta f_m(u_L^+, y, \tau) = \frac{\langle f_m^+(u_L^+, y, \tau)\rangle - \langle f_m^+(u_L^+ = 0, y, \tau = 0)\rangle}{\langle f_m^+(u_L^+ = 0, y, \tau = 0)\rangle} \times 100. \tag{6.4}$$

Figure 9(*a*) show contours of $\Delta u_S^2(u_L^+, y, \tau)$ for $u_L^+ = 2$ (top) and $u_L^+ = -2$ (bottom). Figure 9(*b*) reveals contours of $\Delta u_S^2(u_L^+, y, \tau)$ for different phase lags $\tau U_\infty/\delta = -1$

(left), 0 (middle) and 1 (right). These temporal locations are marked with vertical black lines in figure 9(*a*). It must be noted that the contours for $\tau U_\infty/\delta = 0$ are identical to those in figure 6(*a*). Figure 9 shows an inclined structure that indicates that the amplitude attenuation for negative u_L^+ and the amplitude amplification for positive u_L^+ lag the large-scale fluctuation till the middle of the log region, and this lag increases with increasing wall-normal location. Beyond this location, the amplitude difference goes through zero and becomes positive. However, the maximum positive difference occurs for a positive time shift and this shift decreases with increasing wall-normal location. The figure also shows that the time shift appears to be a constant across all values of u_L^+. This is explored in greater detail later in this section. The general trends in figure 9 are consistent with the phase difference observed by Bandyopadhyay & Hussain (1984) and more recently by Chung & McKeon (2010). This is also consistent with the results of Hutchins *et al.* (2011), who found that the amplitude of the small scales remains in phase (or similarly out of phase) with the streamwise gradient of large-scale fluctuation ($\partial u_L/\partial x$).

Figure 10(*a*) show contours of $\Delta f_m(u_L^+, y, \tau)$ for $u_L^+ = 2$ (top) and $u_L^+ = -2$ (bottom). Figure 10(*b*) reveals contours of $\Delta f_m(u_L^+, y, \tau)$ for different time shifts, $\tau U_\infty/\delta = -1$ (left), 0 (middle) and 1 (right). These temporal locations are marked with vertical black lines in figure 10(*a*), and it is noted that the contours for $\tau U_\infty/\delta = 0$ are identical to those in figure 8(*a*). The contours in figure 10 are seen to be markedly different from the contours in figure 9, suggesting that the temporal shifts in frequency modulation are very different to amplitude modulation. The contours reveal that there is a time delay between the increased or decreased frequency of the small scales and the strength of the large scales. The peak in Δf_m appears to be at around $\tau U_\infty/\delta = -0.2$ in the near-wall region. This time delay is explored in greater detail later in this section. It can also be seen that the frequency modulation effect is diminished beyond $y^+ = 100$ over all time shifts. This is consistent with the observations in the previous section.

The phase lag of amplitude and frequency modulation can be further examined by extracting the time shifts at which the absolute values of Δu_S^2 and Δf_m attain a maximum. This phase lag is determined at each wall-normal location for various values of u_L^+. Figures 11(*a*) and 11(*b*) show the time shifts over a range of wall-normal locations at which Δu_S^2 and Δf_m attain a maximum for different values of u_L^+, respectively. The time shift for amplitude modulation is negative and it decreases with increasing wall-normal distance until the middle of the log region (i.e. up to $y^+ \approx \sqrt{15Re_\tau}$). Beyond this location, the temporal shift is positive and the shift decreases with increasing distance from the wall. The time shifts for amplitude modulation appear to remain constant at a given wall-normal location over all values of u_L^+. This suggests that the phase difference between the large-scale fluctuation and the small scales does not depend on the strength of the large-scale fluctuation. It must be noted that farther away from the wall the data are scattered, especially for intense large-scale fluctuations, due to lack of statistical convergence.

The time shift for frequency modulation is approximately $-0.2\delta/U_\infty$ in the near-wall region, and this delay decreases, reaching zero at around $y^+ = 100$. Beyond this location, the time shift data are scattered. This is mostly due to the fact that there is very limited (or no) frequency modulation in the outer region. Just as in amplitude modulation, the time shifts appear to remain constant at a given wall-normal location over all values of u_L^+. It must be noted that, in the near-wall region, the time shift for frequency modulation is comparable to that for amplitude modulation. A high local shear, correlated with positive u_L^+, results in higher vorticity and consequently higher

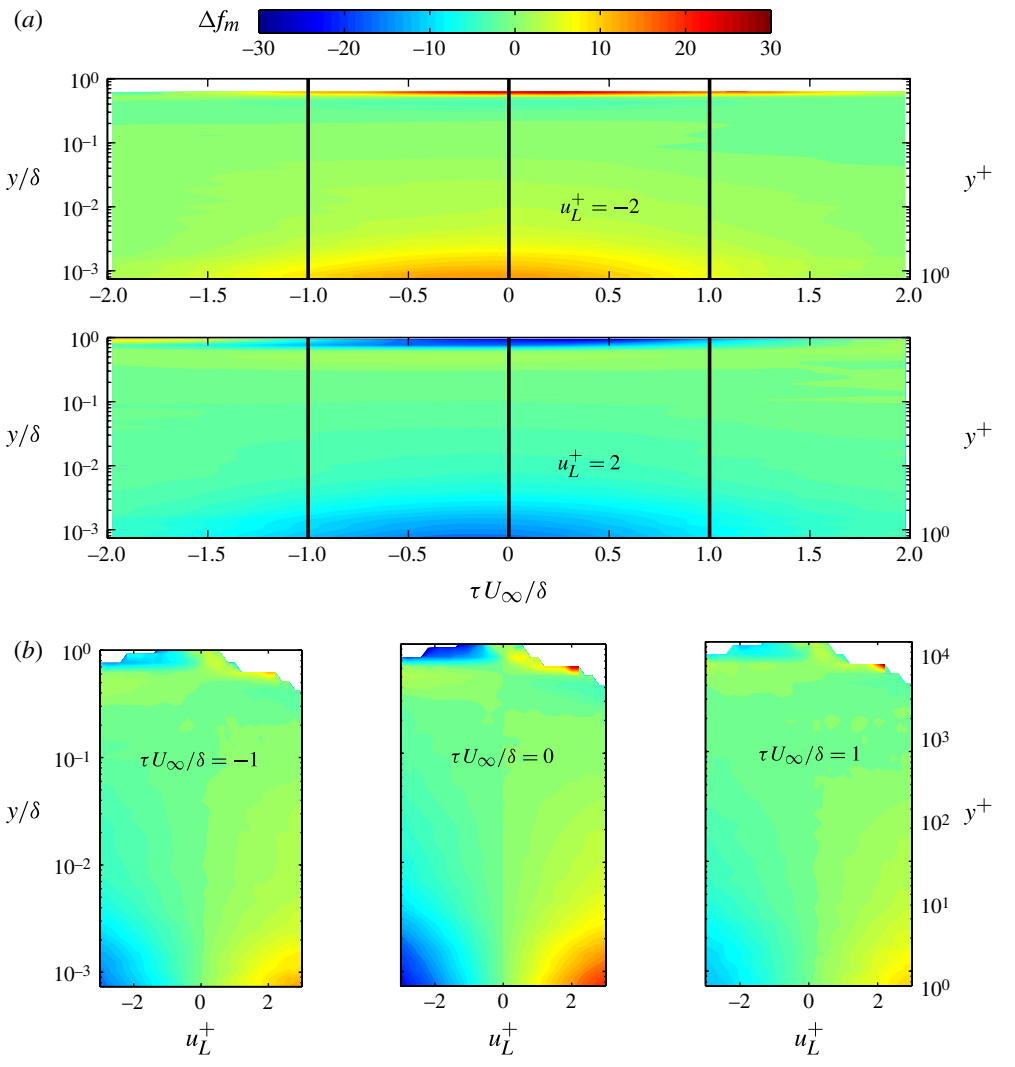

FIGURE 10. (*a*) The top plot show Δf_m as a function of phase lag (τ) and wall-normal location (y) for $u_L^+ = -2$; and the bottom plot shows $\Delta f_m(\tau, y)$ for $u_L^+ = 2$. (*b*) The three plots show Δf_m as a function of u_L^+ and wall-normal location at three different phase-lags, $\tau U_\infty/\delta = -1, 0$ and 1.

amplitude and frequency for the small scales compared to $u_L^+ = 0$. On the other hand, a low value of shear, correlated with negative u_L^+, suppresses the generation of smaller scales, resulting in lower amplitude or frequency. Farther away from the wall (i.e. in the log region), shear is much smaller, since the mean shear decreases dramatically (i.e. $\partial U^+/\partial y^+ \propto 1/y^+$) and therefore the extent of frequency modulation diminishes rapidly farther away from the wall.

7. Spectral analysis: overall modulation effects

In previous sections, the effects of amplitude and frequency modulation were explored separately. However, it would be useful to be able to represent the combined

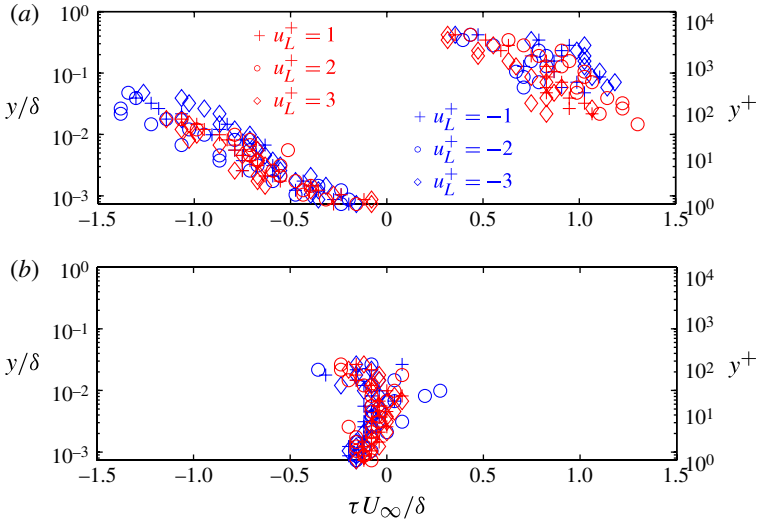

FIGURE 11. Phase lag as a function of wall-normal location for both (*a*) amplitude modulation and (*b*) frequency modulation. The phase lag for amplitude or frequency modulation is determined as the lag at which the absolute value of $\Delta u_S^2/\Delta f_m$ is a maximum at a given wall-normal location.

effect. The combined effects of amplitude and frequency modulation can be captured by examining the conditional spectra of the small-scale fluctuations conditioned on the large-scale fluctuation. This is analogous to computing the short-time correlation, as done by Bandyopadhyay & Hussain (1984), Chung & McKeon (2010) and Guala *et al.* (2011); however, we present the results as a function of u_L^+. It must be noted that this spectral analysis will not capture the phase difference between the large and small scales identified in the previous section.

The procedure to compute the conditional spectrum of the small scales is similar to the procedure outlined in the preceding sections, and is as follows.

(i) The velocity fluctuation (u) is separated into large-scale (u_L) and small-scale (u_S) fluctuations by using a spectral filter of length $\lambda_t U_\infty/\delta = 2$.

(ii) Equally spaced bins with a spacing of 0.2 ranging from $u_L^+ = -6$ to $u_L^+ = 6$ are created for the large-scale fluctuations.

(iii) The time series of both the large- and small-scale fluctuations are divided into individual segments of length $\lambda_t U_\infty/\delta = 2$ (which is the filter time scale that delineates the large scale from the small scales).

(iv) The representative value of the large-scale fluctuation (u_L^+) in a segment is chosen as the value at the centre of an individual segment.

(v) The small-scale signal, $u_S^+(t)$, within the same segment is used to compute the pre-multiplied energy spectrum, where the maximum frequency obtained is determined by the sampling frequency (one-half of the sampling frequency) while the minimum frequency captured is $\lambda_t/2$.

(vi) This spectrum is assigned to the bin corresponding to the value of large-scale fluctuation.

(vii) Steps (iv)–(vi) are repeated for all segments across all wall-normal locations.

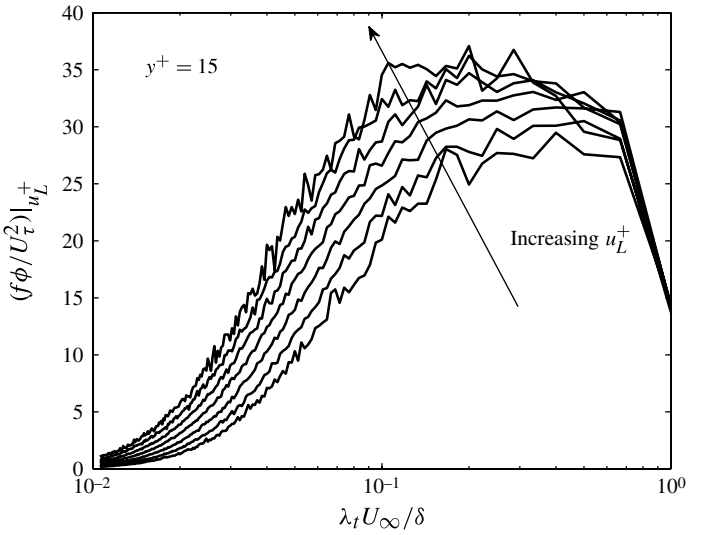

FIGURE 12. Pre-multiplied conditional energy spectra of the small scales as a function of time scale ($\lambda_t = 1/f$) at $y^+ = 15$. The vertical axis shows $f\phi(f)/U_\tau^2|_{u_L^+}$. The various lines show the pre-multiplied conditional spectra of the small scales for $u_L^+ = -3, \ -2, \ -1, \ 0, \ 1, \ 2$ and 3.

(viii) A mean conditional spectrum over the samples in every bin is calculated and this represents a conditional energy spectrum of the small scales conditioned on the value of large-scale fluctuation.

Figure 12 shows pre-multiplied conditional energy spectra of the small scales conditioned on the value of the large-scale fluctuation at $y^+ = 15$. The spectra for $u_L^+ = -3, \ -2, \ -1, \ 0, \ 1, \ 2$ and 3 are shown in the figure. It can be seen that the peak value of the pre-multiplied spectrum increases with increasing value of u_L^+ (as you go from negative u_L^+ to positive u_L^+). This is the spectral manifestation of amplitude modulation where the energy content in the small scales increases with increasing value of the large-scale fluctuation. In addition, it can be seen in figure 12 that the location of the maximum (i.e. time scale band of maximum energy) appears to decrease with increasing value of u_L^+. The changing location of the peak is an indication of frequency modulation where the frequency of small scales with the highest energy content increases with increasing large-scale fluctuation. This is consistent with the observations in the previous sections, and the current result is a spectral representation of frequency modulation. Therefore, the conditional energy spectrum of the small scales provides information on both amplitude and frequency modulation effects. The combined effect of amplitude modulation (i.e. higher overall energy content in the smaller scales) and frequency modulation (i.e. higher and higher frequencies contain more energy) manifests as higher or lower dissipation depending on the value of u_L^+. Indeed, Guala *et al.* (2011) found that dissipation is locally higher for positive u_L^+ and lower for negative u_L^+ in the near-wall region.

8. Discussion

In the previous sections, the effects of both amplitude and frequency modulation of the small scales by the large-scale structures was established. The extent of modulation

varies with distance from the wall. In the near-wall region, amplitude modulation of up to $\pm 30\,\%$ is observed and its extent is higher for higher values of large-scale fluctuation. Amplitude modulation also exhibits a phase difference, indicating that the small scales are amplified a given time delay after the occurrence of the large-scale fluctuation. This time delay increases with increasing wall-normal distance. The frequency modulation effect appears to be confined to the near-wall region, with the effect diminishing rapidly for $y^+ > 100$. Frequency modulation also exhibits a time delay, where the frequency of the small scales is increased or decreased after the occurrence of the large-scale fluctuation, but this delay remains a constant across all wall-normal locations. It is useful at this point to reiterate that the true modulation of frequency and amplitude (in the strictest definition of the large-scale structure actively steering the small-scale behaviour) may be confined to the near-wall region ($y^+ < 100$). Beyond this region, the correlation (and phase shift) between the large-scale fluctuations and small-scale amplitude may be more indicative of a preferential arrangement between these two scales rather than a true modulating influence exerted by the large scales.

An overall summary of the key results in this paper is schematically presented in figure 13. The upper plot gives a kinematic overview across the entire boundary layer. This plot utilizes the knowledge gained about the structure of boundary layers from the broader literature. The plot shows alternating large-scale low- and high-speed forward-leaning structures that are consistent both with observations of superstructure-type events (Chung & McKeon 2010; Hutchins *et al.* 2011) and with the hairpin packet paradigm (Adrian, Meinhart & Tomkins 2000). Meinhart & Adrian (1995), Adrian *et al.* (2000) and Tomkins & Adrian (2003) show that these large-scale uniform momentum regions are separated by vortical structures that exist as a result of the shear layer between high- and low-speed events. The clockwise patterns in the plot indicate increased vorticity contribution above the mean, and anticlockwise indicate a reduced contribution to mean vorticity. In this physical representation, the only true modulation occurs close to the wall due to the modified velocity gradient imposed by the large scales onto the near-wall cycle. The temporal dynamics of amplitude and frequency modulation in the near-wall region is represented in detail in the bottom plot in figure 13. This plot is depicted in the frame of reference of the small scales, i.e. the small scales are stationary while the large-scale structure convects through at a relative convection velocity of $U_{RCLS} = U_{LC} - U_{SC}$ (where U_{LC} and U_{SC} are the convection velocities of large- and small-scale motions).

In the near-wall region, as the large-scale high-speed structure convects through the small scales, the small scales experience a sudden change in velocity. This change, which is a velocity gradient, induces a higher shear stress compared to the mean flow – see Hutchins *et al.* (2011) (the conditional mean profiles from that paper are reproduced as figure 14*a*). This increase in the local skin friction, i.e. an increase in the local Reynolds number, results in an increase in the frequency of the small scales as shown in figure 13. This change in frequency reaches a maximum after a time delay of approximately $0.2\delta/U_\infty$ (as seen in figure 11*b*). This delay is equivalent to the turnover time of the near-wall cycle (i.e. $\tau^+ \approx 100$). This phase difference (or time delay) for frequency modulation remains relatively unchanged across wall-normal locations (in the near-wall region), as seen in figure 11(*b*). It must also be noted that the time delay to achieve maximum amplitude modulation in the near-wall region is comparable to that of frequency modulation, as seen in figure 11(*a*). This is primarily because both amplitude and frequency modulation are a response of the small scales to a sudden change in large-scale velocity (i.e. large-scale velocity gradient). This is

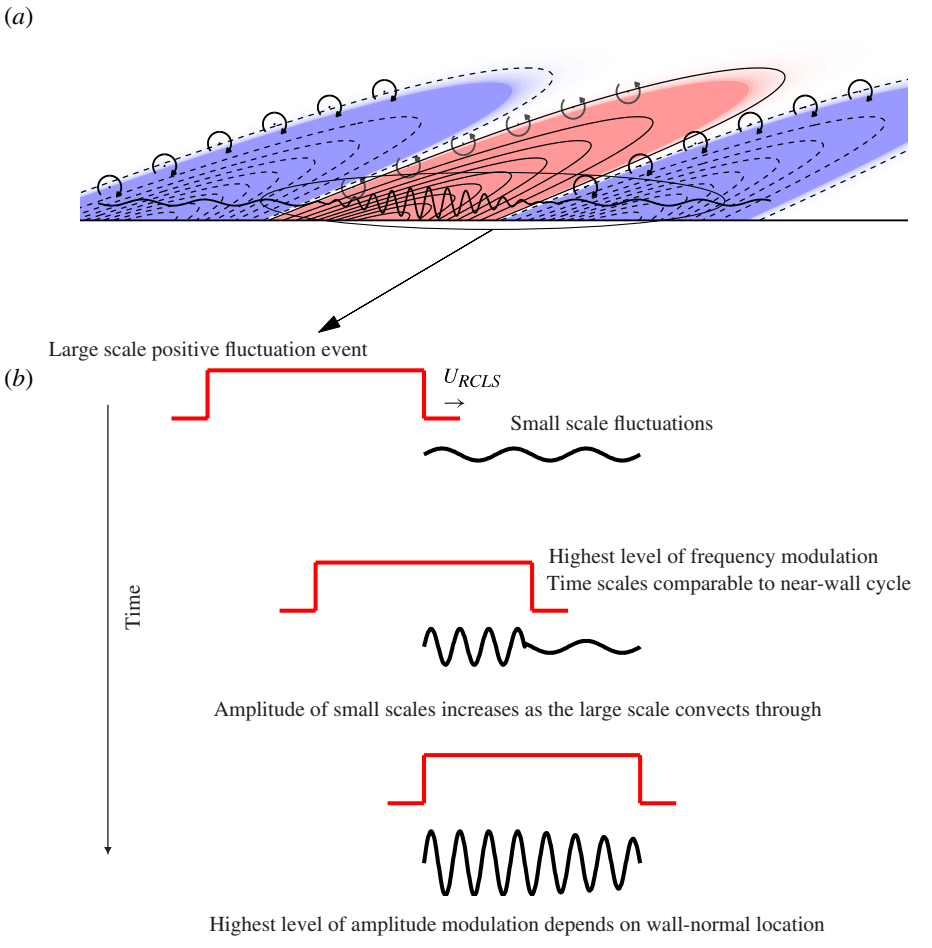

FIGURE 13. (*a*) An overall kinematic representation of amplitude and frequency modulation. The solid contours (red middle area) represent a large-scale high-speed region. The dashed contours (two blue outer areas) indicate a large-scale low-speed region. Arrows represent vorticity fluctuation due to the shear layer between high- and low-speed events (clockwise indicating increased vorticity contribution above the mean, anticlockwise indicating a reduced contribution to mean vorticity). The synthetic velocity trace (thicker solid black line) illustrates the amplitude and frequency modulation of the small-scale eddies in the near-wall cycle. (*b*) A schematic representation that illustrates the temporal dynamics of amplitude and frequency modulation of the small scales by a large-scale high-speed event in the near-wall region (i.e. $y^+ < 100$). The schematic is shown in the frame of reference of the small scales (therefore, they are stationary) as the large-scale high-speed structure convects through with a relative convection velocity of $U_{RCLS} = U_{LC} - U_{SC}$, where U_{LC} and U_{SC} are the convection velocities of large- and small-scale motions.

consistent with a scenario where small scales are generated by the footprint of the large high-speed structure (i.e. the high shear compared to the mean flow) and the time taken for this process to be completed is equivalent to the time scale of the near-wall cycle.

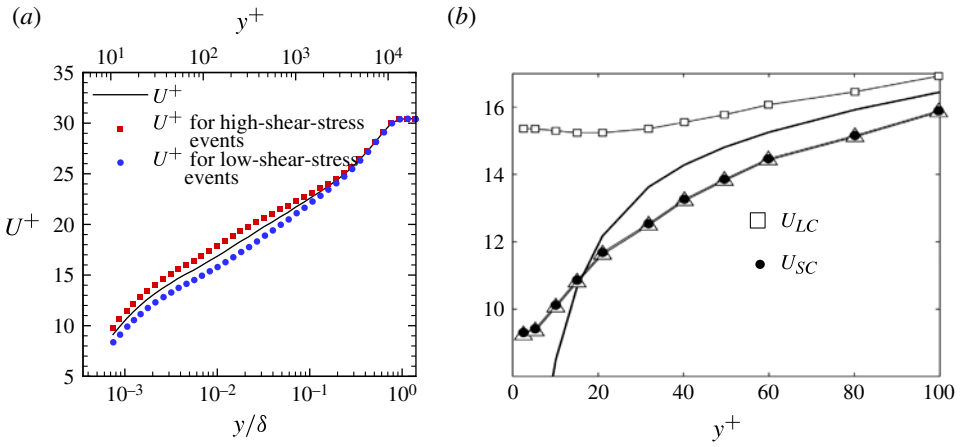

FIGURE 14. (*a*) Unconditional (—) and conditionally averaged mean velocity profiles on low- (○) and high-shear-stress (□) events. This shows the near-wall impact of the large-scale positive and negative velocity fluctuations. (*b*) Convection velocity of the large- and small-scale motions in a turbulent channel flow (reproduced from Del Álamo & Jiménez 2009). The figure shows that the convection velocity of the large scales relative to the small scales, $U_{RCLS} = U_{LC} - U_{SC}$, decreases with increasing wall-normal location. Although the current study is concerned with turbulent boundary layers, the convection velocities are expected to follow a similar trend.

Farther away from the wall, the shear induced by the large-scale structure is comparable to that of the mean flow – see Hutchins *et al.* (2011) and figure 14*a*, which shows that the mean profile conditioned on the existence of a high-shear-stress event at the wall has the same slope as the unconditional mean profile in the log region. Therefore, the frequency of the small scales remains relatively unchanged in the outer region as observed in the previous sections. However, amplitude modulation persists and it demonstrates an increasing phase difference (or time delay) with distance from the wall as seen in figure 11(*a*). This feature can be explained through two possible scenarios, both of which are consistent with the physical model presented in figure 13. First, the increasing phase difference could be the change in the convection velocity of the large scale relative to the small scales (U_{RCLS}) with wall-normal location. Evidence presented in Del Álamo & Jiménez (2009) for a turbulent channel flow (figure 4 in their paper, which is reproduced as figure 14*b*) shows that the difference between the convection velocity of the large scales and the small scales decreases with increasing wall-normal location. Therefore, for a given length scale of the large high-speed structure (say L), the time taken for the large structure to convect past the small scales (L/U_{RCLS}) will increase with increasing wall-normal distance. This will manifest itself as an increase in phase difference with wall-normal location for amplitude modulation. An alternative interpretation for the phase difference in amplitude modulation is provided by the top plot in figure 13. The increasing phase difference can be considered as a manifestation of the preferential spatial arrangement of small-scale vortical activity within the inclined shear layers separating the large-scale high- and low-speed regions. In time-series data (such as those presented in the current study), this preferential arrangement will result in a phase difference between large-scale and small-scale motions.

The physical model shown in figure 13 reconciles a near-wall cycle, the amplitude and frequency of which are believed to scale on the skin friction at the wall, and the packet model of inclined vorticity-rich shear layers separating inclined uniform momentum zones. The schematic explains why the frequency modulation would be confined to the near-wall region, while also providing an explanation for the increasing phase difference with distance from the wall for the amplitude modulation. Given that the magnitude of the large-scale fluctuations increases with Reynolds number, and given that these large-scale fluctuations modulate the amplitude and frequency of the near-wall cycle, it seems reasonable to assume that both modulation effects will strengthen with Reynolds number.

9. Conclusions

In this study we examined the impact of the strength of the large-scale fluctuation on the small scales in wall-bounded turbulence. Time series of hot-wire data were decomposed into large- and small-scale components using a spectral filter of a given length (in this case, $\lambda_t U_\infty/\delta = 2$), and the impact of the large-scale signal on the small scales was examined. The large-scale signals were separated into individual bins of different values ranging from strong negative fluctuation to strong positive fluctuation. The small-scale signals within these large-scale bins were analysed to examine both amplitude and frequency modulation of the small scales by the large scales.

The amplitude of the small scales was computed as the mean square of the small-scale signal within the given filter length. It was shown that this small-scale amplitude increases with increasing value of the large-scale fluctuation (from negative to positive) in the near-wall regions, whereas farther away from the wall the small-scale amplitude decreases with increasing large-scale fluctuation. This clearly reveals that the amplitude modulation effect increases with increasing strength of the large-scale fluctuation. However, the rate of increase in small-scale amplitude with the strength of large-scale signal is nonlinear. The increase in amplitude of small scales for positive values of large-scale fluctuation is not as high as the attenuation of the small-scale amplitude for comparable negative values of large-scale fluctuation.

A new analysis method that counts the number of occurrences of local maxima or minima in the small-scale signal was used to examine frequency modulation effects. The mean separation in time between maxima and minima was used to infer the localized frequency of the small scales. The number of local maxima or minima is conditionally averaged based on the value of the large-scale fluctuation. It was shown that frequency (i.e. number of local maxima or minima) is higher for positive large-scale fluctuations, while it is lower for negative large-scale fluctuations, indicating the presence of frequency modulation. This frequency modulation effect is largely restricted to the near-wall region ($y^+ < 100$).

A phase difference between the large and small scales, in terms of amplitude modulation, was also identified, which is in agreement with previous studies (Bandyopadhyay & Hussain 1984; Chung & McKeon 2010; Hutchins *et al.* 2011). The time shifts for amplitude modulation appear to remain constant at a given wall-normal location over all values of u_L^+. This suggests that the phase difference between the large-scale fluctuation and the small scales does not depend on the strength of the large-scale fluctuation. The phase difference between large and small scales is

markedly different for frequency modulation when compared to amplitude modulation. The phase lag for frequency modulation appears to be much smaller compared to amplitude modulation and does not have the characteristics of an inclined structure. This suggests that the frequency modulation observed in the near-wall region is perhaps a result of local changes in shear and is not necessarily dependent on the overall spatio-temporal structure of the large scales.

The combined effect of both amplitude and frequency modulation was considered by computing conditional spectra of the small-scale signal conditioned on the value of large-scale fluctuation. In the near-wall region, the results indicate that the peak value of the pre-multiplied spectra increases with increasing value of large-scale fluctuation, indicating amplitude modulation, while the frequency at which this peak occurs also increases with increasing value of large-scale signal, revealing frequency modulation. The overall trends observed from the conditional spectra are consistent with the results obtained through statistical analyses.

Finally, a physical mechanism that can reconcile the observations made in the current study is also presented. This mechanism consists of very large-scale motions, consistent with hairpin packet-type models. The footprint from these features imposes a large-scale modulation of the near-wall velocity gradient, which in turn modulates the amplitude and frequency of the near-wall cycle.

Acknowledgements

B.G. acknowledges the support from the European Research Council under the European Union's Seventh Framework Programme (FP7/2007–2013)/ERC Grant agreement No. 277472. D.C.'s research was carried out at the Jet Propulsion Laboratory, California Institute of Technology, under a contract with the National Aeronautics and Space Administration. N.H., J.P.M. and I.M. acknowledge support from the Australian Research Council.

Appendix A. Validation of analysis tools with synthetic signals

In this appendix, we use synthetic signals to show that amplitude and frequency modulation are not artefacts of the data processing tools, but are intrinsic features of the turbulent wall flow.

Synthetic signals are generated using the original hot-wire signals. The original signal is first transformed to the Fourier domain and its amplitude is retained. The phase information of the original signal is discarded and a new phase angle is generated for each Fourier coefficient by randomly generating a number between $-\pi$ and π. The signal with the new phase information is transformed back to the time domain, which is then used to carry out further analysis.

Figure 15(*a*) shows a trace from the original hot-wire signal and the corresponding synthetic signal. On first glance, both time traces appear to be 'turbulent'. Since the amplitude of the synthetic signal is identical to the amplitude of the original signal for each Fourier coefficient, the turbulence intensity as well as the energy spectra obtained from the synthetic data are identical to those of the original hot-wire data. However, the scrambled phase information should remove any correlation that may exist between the large and small scales in the flow. Therefore, these synthetic data can be used to ascertain if the amplitude and frequency modulation analysis presented in the paper are artefacts of the mathematical tools used.

Figures 15(*b*) and 15(*c*) show contours of $\langle u_S^{2+} \rangle$ and $\langle f_m^+ \rangle$ as a function of u_L^+ and wall-normal location for the synthetic signals. It can be seen that the amplitude and

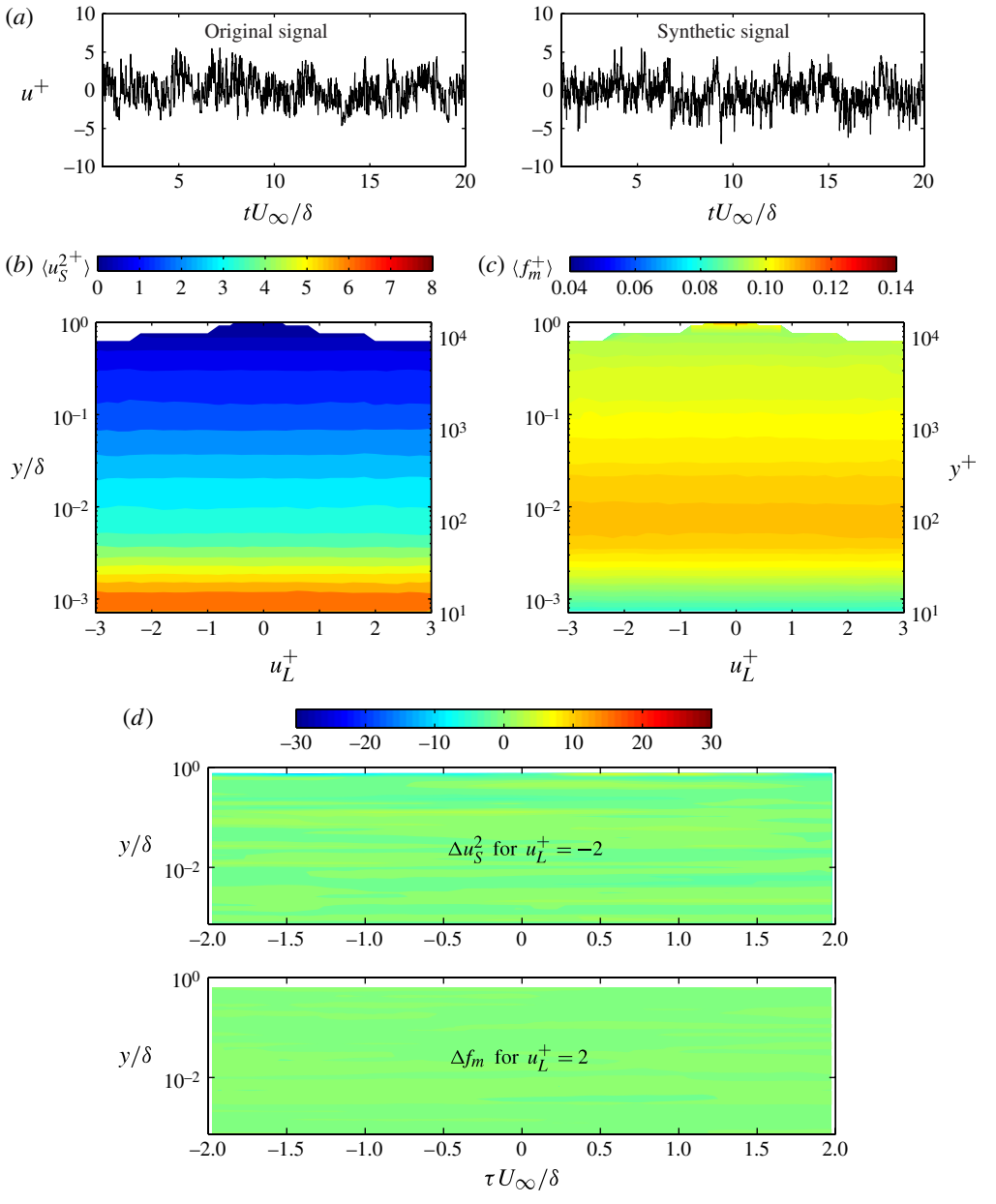

FIGURE 15. (*a*) Instantaneous sample of original and synthetic signals at $y^+ = 15$. Plots of (*b*) $\langle u_S^{2+}\rangle$ and (*c*) $\langle f_m^+\rangle$ as a function of u_L^+ and wall-normal location. (*d*) Plots of Δu_S^2 for $u_L^+ = -2$ and Δf_m^+ for $u_L^+ = 2$ as a function of phase lag (τ) and wall-normal location. The data presented in panels (*b–d*) are calculated using the synthetic signal. The large- and small-scale fluctuations are calculated from the synthetic signal based on a filter time scale of $\lambda_t U_\infty/\delta = 2$ (this filter scale is identical to the one used to analyse the original data in this paper).

the frequency across all values of u_L^+ are equal to each other. This shows that there is no measurable amplitude or frequency modulation in the synthetic signals. Also, the contours in these two figures are markedly different from the corresponding contours in figures 5(*a*) and 7(*a*), which are evaluated using the original signal, indicating that the observed amplitude and frequency modulation are indeed intrinsic features of the flow.

Figure 15(*d*) shows $\Delta u_S^2(u_L^+, y, \tau)$ and $\Delta f_m(u_L^+, y, \tau)$ from different u_L^+ bins. The contours for Δu_S^2 are taken from the bin corresponding to $u_L^+ = -2$, and the contours for Δf_m^+ are from the $u_L^+ = 2$ bin. It can seen that both $\Delta u_S^2(u_L^+ = -2, y, \tau)$ and $\Delta f_m(u_L^+ = 2, y, \tau)$ are essentially zero for all time delays. The bins of u_L^+ in figure 15(*d*) are only chosen as an example. In fact, Δu_S^2 and Δf_m are zero across all time delays for all bins of u_L^+. This further shows that the amplitude and frequency modulation is an intrinsic feature of the flow and is not an artefact of the processing tools.

The results in this appendix are consistent with the validation carried out using synthetic signals in Mathis *et al.* (2009).

Appendix B. Filter scale effects on amplitude or frequency modulation

All the results presented in this paper used the data based on a filter time scale of $\lambda_t U_\infty/\delta = 2$. This filter scale was chosen as it appears to clearly demarcate the high-energy lobe in the near-wall region from the high-energy lobe in the outer region.

In this appendix, we show the effect of this filter time scale on amplitude and frequency modulation. We consider five different filter time scales, between the inner and outer high-energy lobes seen in figure 1. The five vertical lines at $\lambda_t U_\infty/\delta = 0.5,\ 1,\ 2,\ 4$ and 6 as shown in figure 1 are used as filter time scales. Figure 16 shows the effect of these different filters on amplitude and frequency modulation. The large- and small-scale fluctuations are computed as outlined in § 3.1 for each filter case. The figures in the left column show Δu_S^2 and the figures in the right column show Δf_m, respectively, for various filter time scales. The filter time scales are indicated in the figure. As the filter time scale increases, the number of data samples within higher values of u_L^+ decreases, and consequently we encounter statistical convergence issues. Despite this issue, the general trends of amplitude and frequency modulation can still be observed.

For amplitude modulation (left column), it is observed that near the wall the amplitude of the small scales is attenuated for $u_L^+ < 0$ and amplified for $u_L^+ > 0$. Also, the location where the modulation effect experiences a change in behaviour (i.e. going from amplification to attenuation for $u_L^+ > 0$) appears to remain unchanged with increasing filter time scale. This is consistent with the results of Mathis *et al.* (2009), who found that the correlation between the large-scale fluctuation and the envelope of the small scales is only weakly dependent on the filter.

For frequency modulation (right column), we observe that the filter scale does not alter the general trends, and the location where frequency modulation effects diminish ($y/\delta \approx 0.1$) does not appear to change with increasing filter scale. This suggests that the general trends of amplitude and frequency modulation noted in this study only weakly depend on the choice of the filter time scale. Obviously, the essential requirement is the presence of separation of scales between the large and small scales, which will enable us to decompose the fluctuations.

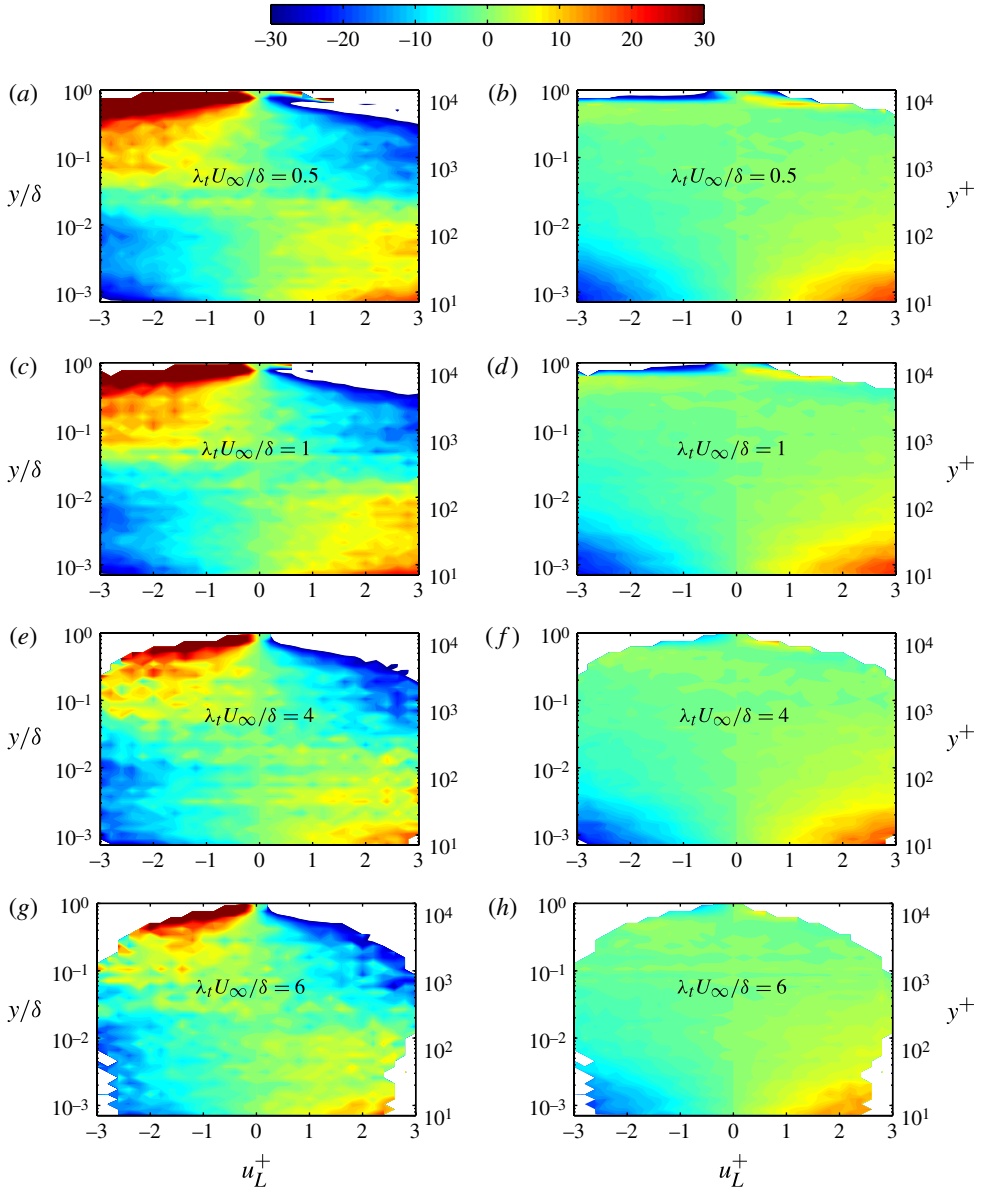

FIGURE 16. Effect of filter time scale on amplitude and frequency modulation. The left and right columns show Δu_S^2 and Δf_m, respectively, for filter length $\lambda_t U_\infty/\delta = 0.5$, 1, 4 and 6 (as shown). The blank regions for extreme values of u_L^+ indicate lack of statistical convergence.

REFERENCES

ADRIAN, R. J., MEINHART, C. D. & TOMKINS, C. D. 2000 Vortex organization in the outer region of the turbulent boundary layer. *J. Fluid Mech.* **422**, 1–53.

BAILEY, S. C. C., HULTMARK, M., SMITS, A. & SCHULTZ, M. P. 2008 Azimuthal structure of turbulence in high Reynolds number pipe flow. *J. Fluid Mech.* **615**, 121–138.

BANDYOPADHYAY, P. R. & HUSSAIN, A. K. M. F. 1984 The coupling between scales in shear flows. *Phys. Fluids* **27** (9), 2221–2228.

BERNARDINI, M. & PIROZZOLI, S. 2011 Inner/outer layer interactions in turbulent boundary layers: a refined measure for the large-scale amplitude modulation mechanism. *Phys. Fluids* **23** (6), 061701.

BLACKWELDER, R. F. & KOVASZNAY, L. S. G. 1972 Time scales and correlations in a turbulent boundary layer. *Phys. Fluids* **15**, 1545–1554.

BROWN, G. R. & THOMAS, A. S. W. 1977 Large structure in a turbulent boundary layer. *Phys. Fluids* **20**, S243–S251.

CHUNG, D. & MCKEON, B. J. 2010 Large-eddy simulation of large-scale structures in long channel flow. *J. Fluid Mech.* **661**, 341–364.

CLAUSER, F. H. 1956 The turbulent boundary layer. *Adv. Mech.* **4**, 1–51.

DEL ÁLAMO, J. C. & JIMÉNEZ, J. 2003 Spectra of the very large anisotropic scales in turbulent channels. *Phys. Fluids* **15** (6), L41–L44.

DEL ÁLAMO, J. C. & JIMÉNEZ, J. 2009 Estimation of turbulent convection velocities and corrections to Taylor's approximation. *J. Fluid Mech.* **640**, 5–26.

DENNIS, D. J. C. & NICKELS, T. B. 2008 On the limitations of Taylor's hypothesis in constructing long structures in a turbulent boundary layer. *J. Fluid Mech.* **614**, 197–206.

GANAPATHISUBRAMANI, B., LONGMIRE, E. K. & MARUSIC, I. 2003 Characteristics of vortex packets in turbulent boundary layers. *J. Fluid Mech.* **478**, 35–46.

GUALA, M., HOMMEMA, S. E. & ADRIAN, R. J. 2006 Large-scale and very-large-scale motions in turbulent pipe flow. *J. Fluid Mech.* **554**, 521–542.

GUALA, M., METZGER, M. & MCKEON, B. J. 2011 Interactions within the turbulent boundary layer at high Reynolds number. *J. Fluid Mech.* **666**, 573–604.

HUNT, J. C. R. & MORRISON, J. F. 2000 Eddy structure in turbulent boundary layers. *Eur. J. Mech (*B/*Fluids)* **19**, 673–694.

HUTCHINS, N. & MARUSIC, I. 2007*a* Evidence of very long meandering structures in the logarithmic region of turbulent boundary layers. *J. Fluid Mech.* **579**, 1–28.

HUTCHINS, N. & MARUSIC, I. 2007*b* Large-scale influences in near-wall turbulence. *Phil. Trans. R. Soc. Lond.* **365**, 647–664.

HUTCHINS, N., MONTY, J. P., GANAPATHISUBRAMANI, B., NG, H. & MARUSIC, I. 2011 Three-dimensional conditional structure of a high Reynolds number turbulent boundary layer. *J. Fluid Mech.* **673**, 255–285.

HUTCHINS, N., NICKELS, T. B., MARUSIC, I. & CHONG, M. S. 2009 Hot-wire spatial resolution issues in wall-bounded turbulence. *J. Fluid Mech.* **632**, 431–442.

KAILASHNATH, K. & SREENIVASAN, K. R. 1993 Zero crossings of velocity fluctuations in turbulent boundary layers. *Phys. Fluids* **5** (11), 2879–2885.

KIM, K. C. & ADRIAN, R. J. 1999 Very large-scale motion in the outer layer. *Phys. Fluids* **11** (2), 417–422.

KOVASZNAY, L. S. G., KIBENS, V. & BLACKWELDER, R. F. 1970 Large-scale motion in the intermittent region of a turbulent boundary layer. *J. Fluid Mech.* **41**, 283–326.

LIGRANI, P. M. & BRADSHAW, P. 1987 Spatial resolution and measurement of turbulence in the viscous sublayer using subminiature hot-wire probes. *Exp. Fluids* **5**, 407–417.

MARUSIC, I., MATHIS, R. & HUTCHINS, N. 2010 Predictive model for wall-bounded turbulent flow. *Science* **329** (5988), 193–196.

MATHIS, R., HUTCHINS, N. & MARUSIC, I. 2009 Large-scale amplitude modulation of the small-scale structures in turbulent boundary layers. *J. Fluid Mech.* **628**, 311–337.

MATHIS, R., HUTCHINS, N. & MARUSIC, I. 2011 A predictive inner–outer model for streamwise turbulence statistics in wall-bounded flows. *J. Fluid Mech.* **681**, 537–566.

MEINHART, C. D. & ADRIAN, R. J. 1995 On the existence of uniform momentum zones in a turbulent boundary layer. *Phys. Fluids* **7** (4), 694–696.

MONTY, J. P., STEWART, J. A., WILLIAMS, R. C. & CHONG, M. S. 2007 Large-scale features in turbulent pipe and channel flows. *J. Fluid Mech.* **589**, 147–156.

NAGIB, H. & CHAUHAN, K. 2008 Variations of Von Kármán coefficient in canonical flows. *Phys. Fluids* **20**, 101518.

NICKELS, T. B., MARUSIC, I., HAFEZ, S. & CHONG, M. S. 2005 Evidence of the k^{-1} law in high-Reynolds number turbulent boundary layer. *Phys. Rev. Lett.* **95**, 074501.

NICKELS, T. B., MARUSIC, I., HAFEZ, S., HUTCHINS, N. & CHONG, M. S. 2007 Some predictions of the attached eddy model for a high Reynolds number boundary layer. *Phil. Trans. R. Soc. Lond.* **265**, 807–822.

RAO, K. N., NARASIMHA, R. & NARAYANAN, M. A. B. 1971 The phenomenon in a turbulent boundary layer. *J. Fluid Mech.* **48**, 339–352.

REPETTO, M. P. 2005 Cycle counting methods for bi-modal stationary Gaussian processes. *Prob. Engng Mech.* **20** (3), 229–238.

RYCHLIK, I. 1993 Characterisation of random fatigue loads. In *Stochastic Approach to Fatigue* (ed. K Sobczyk), *CISM Courses and Lectures*, vol. 334. Springer.

SCHLATTER, P. & ÖRLÜ, R. 2010 Quantifying the interaction between large and small scales in wall-bounded turbulent flows: a note of caution. *Phys. Fluids* **22**, 051704.

SREENIVASAN, K. R. 1985 On the fine-scale intermittency of turbulence. *J. Fluid Mech.* **151**, 81–103.

SREENIVASAN, K. R., PRABHU, A. & NARASIMHA, R. 1983 Zero-crossings in turbulent signals. *J. Fluid Mech.* **137**, 251–272.

TOMKINS, C. D. & ADRIAN, R. J. 2003 Spanwise structure and scale growth in turbulent boundary layers. *J. Fluid Mech.* **490**, 37–74.

WARK, C. E. & NAGIB, H. M. 1991 Experimental investigation of coherent structures in turbulent boundary layers. *J. Fluid Mech.* **230**, 183–208.